

TRANSIT TIMING OBSERVATIONS FROM *Kepler* : IV. CONFIRMATION OF 4 MULTIPLE PLANET SYSTEMS BY SIMPLE PHYSICAL MODELS

DANIEL C. FABRYCKY^{1,2}, ERIC B. FORD³, JASON H. STEFFEN⁴, JASON F. ROWE^{5,6}, JOSHUA A. CARTER^{7,2}, ALTHEA V. MOORHEAD³, NATALIE M. BATALHA⁸, WILLIAM J. BORUCKI⁶, STEVE BRYSON⁶, LARS A. BUCHHAVE^{18,19}, JESSIE L. CHRISTIANSEN^{5,6}, DAVID R. CIARDI¹⁶, WILLIAM D. COCHRAN¹⁷, MICHAEL ENDL¹⁷, MICHAEL N. FANELLI¹², DEBRA FISCHER¹³, FRANCOIS FRESSIN⁷, JOHN GEARY⁷, MICHAEL R. HAAS⁶, JENNIFER R. HALL⁹, MATTHEW J. HOLMAN⁷, JON M. JENKINS^{5,6}, DAVID G. KOCH⁶, DAVID W. LATHAM⁷, JIE LI^{5,6}, JACK J. LISSAUER⁶, PHILIP LUCAS¹⁰, GEOFFREY W. MARCY¹¹, TSEVI MAZEH²⁰, SEAN MCCAULIFF⁶, SAMUEL QUINN⁷, DARIN RAGOZZINE⁷, DIMITAR SASSELOV⁷, AVI SHPORER^{14,15}

ApJ in press (accepted Jan. 5, 2012)

ABSTRACT

Eighty planetary systems of two or more planets are known to orbit stars other than the Sun. For most, the data can be sufficiently explained by non-interacting Keplerian orbits, so the dynamical interactions of these systems have not been observed. Here we present 4 sets of lightcurves from the *Kepler* spacecraft, which each show multiple planets transiting the same star. Departure of the timing of these transits from strict periodicity indicates the planets are perturbing each other: the observed timing variations match the forcing frequency of the other planet. This confirms that these objects are in the same system. Next we limit their masses to the planetary regime by requiring the system remain stable for astronomical timescales. Finally, we report dynamical fits to the transit times, yielding possible values for the planets' masses and eccentricities. As the timespan of timing data increases, dynamical fits may allow detailed constraints on the systems' architectures, even in cases for which high-precision Doppler follow-up is impractical.

Keywords: planetary systems; stars: individual (KID 10358759 / KOI-738 / Kepler-29; KID 3832474 / KOI-806 / Kepler-30; KID 9347899 / KOI-935 / Kepler-31, KID 9787239 / KOI-952 / Kepler-32); planets and satellites: detection, dynamical evolution and stability; methods: statistical

daniel.fabrycky@gmail.com

¹ Department of Astronomy and Astrophysics, University of California, Santa Cruz, Santa Cruz, CA 95064, USA

² Hubble Fellow

³ Astronomy Department, University of Florida, 211 Bryant Space Sciences Center, Gainesville, FL 32111, USA

⁴ Fermilab Center for Particle Astrophysics, P.O. Box 500, MS 127, Batavia, IL 60510, USA

⁵ SETI Institute, Mountain View, CA, 94043, USA

⁶ NASA Ames Research Center, Moffett Field, CA, 94035, USA

⁷ Harvard-Smithsonian Center for Astrophysics, 60 Garden Street, Cambridge, MA 02138, USA

⁸ San Jose State University, San Jose, CA 95192, USA

⁹ Orbital Sciences Corporation/NASA Ames Research Center, Moffett Field, CA 94035, USA

¹⁰ Centre for Astrophysics Research, University of Hertfordshire, College Lane, Hatfield, AL10 9AB, England

¹¹ University of California, Berkeley, Berkeley, CA 94720

¹² Bay Area Environmental Research Institute/NASA Ames Research Center, Moffett Field, CA 94035, USA

¹³ Astronomy Department, Yale University, New Haven, CT, USA ; Department of Physics and Astronomy, San Francisco State University, San Francisco, CA, USA

¹⁴ Las Cumbres Observatory Global Telescope Network, 6740 Cortona Drive, Suite 102, Santa Barbara, CA 93117, USA

¹⁵ Department of Physics, Broida Hall, University of California, Santa Barbara, CA 93106, USA

¹⁶ NASA Exoplanet Science Institute/Caltech, Pasadena, CA 91126, USA

¹⁷ McDonald Observatory, The University of Texas, Austin TX 78730, USA

¹⁸ Niels Bohr Institute, University of Copenhagen, DK-2100 Copenhagen, Denmark

¹⁹ Centre for Star and Planet Formation, Natural History Museum of Denmark, University of Copenhagen, DK-1350 Copenhagen, Denmark

²⁰ School of Physics and Astronomy, Raymond and Beverly Sackler Faculty of Exact Sciences, Tel Aviv University, Tel Aviv 69978, Israel

1. INTRODUCTION

So far, 170 systems with more than one transiting planet candidate have been discovered by *Kepler* (Borucki et al. 2011), enabling simple dynamical models for an astounding variety of planetary systems (Lissauer et al. 2011b). In particular, two very important dynamical quantities, the planetary period and phase, are measured to high precision by *Kepler*. If we further assume, as is true for the Solar System, that the planets orbit in the same direction, in nearly the same plane, and on nearly circular orbits, then we have a fiducial model that specifies the positions of the planets as a function of time. However, planets do not follow independent Keplerian orbits; instead planets interact with each other gravitationally. These small perturbations to the orbits affect the transit times, which can be calculated via numerical simulations. If the calculated transit timing variations match essential aspects of the observed data, then we obtain independent confirmation that two objects are orbiting the same star.

In this paper, we develop simple physical models and compare them to *Kepler* data to confirm 4 planetary systems, Kepler-29-32. Instead of exhaustively modeling the systems, as has been our practice up until now (Holman et al. 2010; Lissauer et al. 2011a; Cochran et al. 2011), we content ourselves with providing upper limits to the planetary masses, based on the principle that the system is extremely unlikely to be dynamically unstable on timescales much less than the age of the star. Thus, we infer planetary masses for 9 objects in these 4 systems, and deem them planets on this basis. This paper is being published contemporaneously with two companion papers, which explore anticorrelated transit timing variations for the confirmation of pairs of planets, by Ford et al. (2012) (hereafter Paper II) and Steffen et al. (2012) (hereafter Paper III), which together with this paper form a catalog of 10 confirmed systems of multiple-transiting planets.

The organization of this paper is as follows. Section 2 introduces the target stars, describes the transit timing data, and discusses how we assess whether the transit timing signal varies on the theoretically-expected timescale. Section 3.1 applies that methodology to confirm 4 planetary systems, and section 3.2 discusses the identification of their host stars. Section 4 is devoted to constraining the masses of the planets, primarily by dynamical stability, but also via modeling the transit timing signal itself. Section 5 closes with a discussion of these results and a perspective about the future of transit-timing confirmation of multiply-transiting systems with *Kepler*.

2. METHODS

2.1. Determination of Stellar Parameters

Identifying properties of the host stars studied here are in Table 1, e.g., their names in various catalogs.

For stars Kepler-29, Kepler-30, and Kepler-32, we obtained spectra from several different telescopes as part of the *Kepler* team’s regular ground-based follow-up program. Two independent analyses were performed, a standard analysis using ‘Spectroscopy Made Easy’ (Valenti & Piskunov 1996; Valenti & Fischer 2005), as well as a newly-formulated analysis called SPC (Buchhave et al. in prep.), to obtain the parameters T_{eff} , $\log g$,

[Fe/H], and when possible $v \sin i$. For Kepler-31 we did not obtain a spectrum, but instead adopted these values from the *Kepler* input catalog (KIC; Brown et al. 2011) – i.e., based on color photometry – with generous error bars. From these values we performed a Bayesian analysis using Yonsei-Yale stellar isochrones (Yi et al. 2001) to extract best-fit and 68% confidence regions on M_{\star} and R_{\star} (e.g. Pont & Eyer 2004; Takeda et al. 2007). All these values are reported in Table 2.

2.2. Measurement of Transit Times and Parameters

The data we use for this study are long-cadence lightcurves from quarters 1 through 6 (and additionally for Kepler-31 only, quarters 7 and 8), available at the Multimission Archive at STScI (MAST²¹).

For most of the sample, we used timing results from the general-purpose routines of J. Rowe, previously described in Ford et al. (2011) [Paper I]. For Kepler-30b, extremely large variation in the transit times caused the general-purpose algorithm to fail (a linear model for the times of transit incorrectly predicts some observed times by over half a day, see section 3.1.2). Thus, around each transit of this planet, we fit model transit curves (Mandel & Agol 2002) and minimized the sum-of-squared residuals, the standard χ^2 function. We sampled χ^2 over a grid of timing offsets, and fit a parabola to the region within $\Delta\chi^2 \leq 7$ of the minimum value. That parabola thus has a width which is more stable to noise properties than the local curvature is, and we adopt its minimum as the transit time and its width (where $\Delta\chi^2 = 1$) as the error bar.

The transit times for all the planets analyzed herein are given in Table 6.

We also fit transit curves for all our candidates to determine best-fit parameters and errors. The first step was to detrend the lightcurve; we masked out each transit and fit a polynomial over timescales of 1000 minutes and divided the whole lightcurve by it, to obtain a detrended, normalized lightcurve f . Second, we defined a contamination-corrected lightcurve via $f_{\text{corr}} = (f - c)/(1 - c)$, where c is the fractional amount of light leaking into the aperture from known nearby stars, the ‘contamination’ reported on MAST for each target for each quarter. Third, we assembled a phased lightcurve by subtracting the previously-measured transit time from each transit²². We used only non-overlapping transits, for which another planet’s transit center was not within 5 hours²³. To construct a flux value of the long cadence (29.4 min), we took 20 samples evenly spaced over that timespan (using OCCULTSMALL; Mandel & Agol 2002) and averaged them. Finally, we fit the following four parameters: radius ratio R_p/R_{\star} , duration T_{dur} , scaled impact parameter b , and linear limb-darkening coefficient u . The duration is defined as the time between mid-ingress and mid-egress, when the center of the planet passes over

²¹ [\protecthttp://archive.stsci.edu/kepler/](http://archive.stsci.edu/kepler/)

²² For the very small candidates KOI-935.04 and KOI-952.05, individual transit times were not reliably measured (hence they are not included in Table 6), so we used a linear ephemeris for fitting their transit parameters, and held their impact parameters b fixed at 0 and their limb-darkening coefficients u fixed at 0.5.

²³ We also discarded Kepler-31c’s transits near $t - 245000 = 16.8$ and 400.5, as these had corrupted data, apparently due to detrending problems near gaps.

the limb of the star. We report these parameters in Table 3.

As a check on these stellar and planetary parameters, and as a first indication that all the planet candidates in each system are transiting the target stars, we computed for each planet candidate the transit duration that would be obtained by an orbit that is edge-on ($b = 0$) and circular ($e = 0$). These values are plotted against the measured values in Figure 1. We see only a little evidence that these computed values are slightly larger than the measured ones, an indication that either (i) the computed stellar radii are too large or stellar masses are too small, or (ii) the planets’ orbits are systematically seen near pericenter of moderately eccentric orbits, or — most probably — (iii) the planets’ orbits are not quite edge-on ($b \neq 0$).

2.3. Dynamical Expectations and their Observational Confirmation

We begin N-body integrations near the center of the dataset (t [BJD] = 2455220), using coplanar, circular orbits that match the observed periods and transit epochs, and using nominal masses $M_p = M_{\oplus}(R_p/R_{\oplus})^{2.06}$. This set of physical models was introduced by Lissauer et al. (2011b), and it helps us diagnose the most prominent physical interactions. For systems of more than two planets, we break the problem into planet pairs, in an effort to probe the individual interactions. First, we calculate transit times as described by Fabrycky (2010) from the beginning of the dataset until 10 years later. Next, the deviations of those simulated transit times from a linear ephemeris calculated on those times (i.e., the Simulated minus Calculated diagram, $S - C$) is Fourier analyzed to find the dominant frequency (Scargle 1982; Zechmeister & Kürster 2009), which are given in Table 4.

We test for variations at this frequency in the observed timing (i.e., the Observed minus Calculated diagram, $O - C$). The frequency is already determined theoretically (above), but we allow amplitude and phase of the sinusoid and a constant offset to vary freely to fit the data. This approach contrasts to a periodogram search, which tests many frequencies. By fixing this important parameter rather than scanning over it, our method is more sensitive than a periodogram search at finding variations at the predicted frequency. The reason we treat the phase as a free parameter is that it is expected to have a complex dependence on the eccentricities of both the perturbing planet and the perturbed planet. That is, we cannot rely on the values from a model which assumes circular orbits. The same is true for amplitude, which further depends on the masses of the planets, which are not known at this initial stage of modeling. In contrast, the dominant frequency from those models should be present in the data, although perhaps no longer dominant, even if both planets are eccentric or of a mass different than assumed. This test for a TTV periodicity at the predicted frequency may not yield a significant detection if (a) eccentricity significantly changes the character of the variations, or (b) the transit variations are dominated by a non-transiting planet. In these cases, large variations may be present, but have little power at the predicted frequency, so more data-driven methods (papers II and III) are more useful. However, we note that for the systems presented in those papers, the dominant

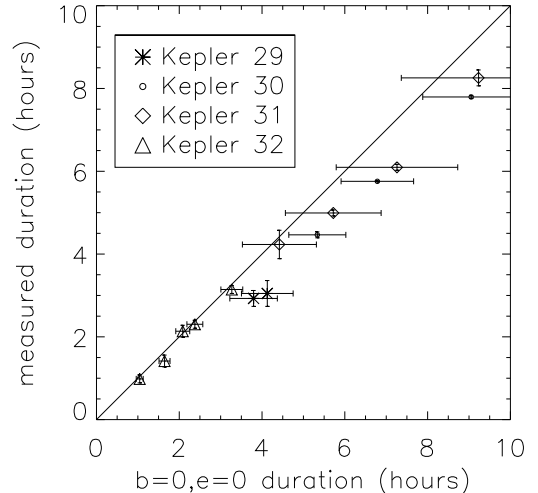


Figure 1. Computed and measured durations of the planet candidates in our sample. The line shows 1:1. The data come close to it, providing a useful check on our interpretation of planetary systems orbiting the targets stars. That the data fall slightly below the line could mean either the stellar parameters or the assumed edge-on and circular orbits are not perfectly correct.

timescale of variation has a simple physical interpretation and is captured by the nominal models described in this paper.

The amplitude of the best-fitting sinusoid at the theorized frequency is recorded, and it is compared to the same calculation for 10^5 realizations of the observational $O - C$ data with scrambled entries. These scrambled datasets should not contain the signal, but they will contain the same distribution of noise (which is possibly non-Gaussian, with outliers). Our criterion for confirmation is that fewer than 100 of these realizations yield larger amplitudes than the real data, i.e., a False Alarm Probability (FAP) of $< 10^{-3}$. Note that our method does not require that *both* planets show a TTV signal with such a low FAP. Even if the transits of one planet are at the limit of detectability, as long as we can establish its orbital period and phase, we have what we need to estimate its dynamical effect on the other planet, whose TTVs must behave as expected. The FAP statistics are reported in Table 4 for the systems confirmed principally via this method (i.e., those of Tables 1-3). Moreover, we present small FAPs reconfirming Kepler-9bc (Holman et al. 2010), Kepler-18cd (Cochran et al. 2011), and nearly all of the systems presented in papers II and III, as these systems show anticorrelated TTVs at the timescale predicted by the nominal models.

3. RESULTS

3.1. Confirmation of Kepler Planets

Here we describe the 4 planetary systems confirmed principally by this method. Where interesting comparisons can be made to other methods (paper II and paper III), we do so. Table 1 gives the catalog properties and Table 2 gives the physical properties of the host stars detailed in this paper.

3.1.1. KOI-738 = Kepler-29

The lightcurve of Kepler-29 is plotted in Figure 2, and the phase curves of the two Neptune-size planets is plotted in Figure 3. Their periods of 10.3376(2) days and 13.2907(4) days form a ratio 1.28566 ± 0.00005 , which lies right at a 9:7 ($= 1.28571$) orbital resonance. Being fractionally closer than 8×10^{-5} of a second-order resonance in this region would happen only 0.5% of the time by chance, and similar for other resonant orders. Being so close to a low-order resonance — consistent with dynamical libration — suggests dynamical interaction helped to establish their orbital architecture. Thus, from the period ratio alone, we have an indication that these objects are in the same system.

Furthermore, since the ratio is not significantly offset from the resonance, the nominal integrations result in an extremely long-timescale variation in $O - C$ (fig. [4]), even slightly longer than the sample 10-year integration used to find it. Therefore, on the timescale of our data, the predicted sinusoid would look only like a quadratic in $O - C$, as is observed (figure 4, left-hand side). The data for the shorter-period planet (Kepler-29b) indicate this quite robustly ($FAP \simeq 0.02\%$) and hint at oppositely-directed curvature for the longer-period planet (Kepler-29c has $FAP \simeq 1.5\%$). On the basis of the former we confirm the system really is composed of two planets.

However, a parabolic signature is not specific enough to uniquely specify the other planet as the perturber, so we carried the investigation one more step. The nominal prediction for year-timescale $O - C$ (figure 4, right-hand side) is not dominated by a parabola, but is instead a “chopping” signal on the frequency at which the planets come back to the same configuration,

$$P_{ttv} = 9 \times 10.3376d = 7 \times 13.2907d = 93d. \quad (1)$$

Thus, we search for that timescale. After subtracting the curvature models shown in figure 4 (left-hand side), we computed the amplitude of the best-fitting sinusoid at the period of equation 1. For Kepler-29b and Kepler-29c, the amplitude was 5 and 12 minutes, respectively, quite similar to that predicted by figure 4. Then we scrambled the data to find a FAP: it was 0.6% and 1.1% for the two planets, respectively. To emphasize this point, we plot in Figure 5 the cross-correlation statistic defined in Paper III: a spike is seen at ~ 90 days, at positive values of Ξ (i.e., anticorrelation at the predicted timescale). Therefore, the signal at the expected chopping timescale is a third, albeit modestly significant, indication that these two objects are really planets in the same system.

3.1.2. KOI-806 = Kepler-30

Kepler-30 is a remarkable system of three planets, all with extremely significant transit timing variations. Its lightcurve is shown in Figure 6 and each planet’s phase curve is shown in Figure 7. A Neptune-size inner planet ($P_b = 29.2$ days) lies just interior to a 2:1 resonance with a Jupiter-size planet ($P_c = 60.3$ days). Their mutual perturbation causes a transit timing variation with a frequency equal to the difference of the orbital frequencies from the resonance:

$$P_{ttv} = 1/|2/60.3d - 1/29.2d| = 900d. \quad (2)$$

Since one of the participating planets has deep transits and thus is presumably massive, the signal is expected to

be large. The theory predicts a sinusoid with a period a bit longer than the data. Indeed, the data show an enormous signal consistent with these expectations (Fig. [8]). Thus, we confirm Kepler-30b and Kepler-30c as objects orbiting the same star.

Since their orbits are spaced a bit wider than the other planets confirmed in this paper, dynamical stability is not as strong a constraint on their masses. We find a mass upper limit (see section 4.1) of about $17 M_{\text{Jup}}$. However, eccentricity can also account for the large transit timing signals, so neither planet is necessarily nearly this massive (in particular, the small-radius Kepler-30b should not be multiple Jupiter masses). The deviations from a constant ephemeris for planet b are roughly parabolic and span from +16 hr to −13 hr, i.e. they span 1.2 days, by far the largest timing variations for a multiple-planet system yet detected (but not quite rivaling the circumbinary planet Kepler-16(AB)b Doyle et al. 2011). However, there is more signal in this TTV curve than just the large parabolic trend. The rising branch of both the observed signal and the theoretical signal show a short-timescale “chopping” effect for Kepler-30b, where the even and odd transits times show structure, due to the 2:1 resonance. A similar effect was seen previously in Kepler-9b (Holman et al. 2010). A mass limit that takes into account the observed transit times will be discussed in section 4.2. It results in a much tighter constraint, but it is less robust because it is not based on an exhaustive exploration of parameter space.

We can also confirm Kepler-30d is likely a planet in the same system, as transit timing variations with a ~ 2 hr timescale are seen in it (fig. 9). However, the interpretation is slightly less clear, as only 4 transits of Kepler-30d ($P = 143.2128$ d) have been recorded so far, so the shape of the variation is poorly determined. This perturbation is anticorrelated with the swing seen in its neighbor (Kepler-30c), but that swing might be predominantly due to Kepler-30c’s near-resonant interaction with Kepler-30b. According to the nominal integration, the timescale for the interaction between planets d and c should be ~ 400 days (Fig. 9 and Table 4), similar to the span of the dataset. When the dataset is doubled, this might be discerned from the longer timescale (eq. 2) interaction between the inner two planets. Even without a detailed analysis, we determine from transit timing that Kepler-30d is an object in the same system. We carry out preliminary transit-timing modeling of the three planets in section 4.2.

Due to the large timing variations and deep transits found in this system, we find it instructive to show individual transits to make several other points. In Figure 10 we plot the transits of Kepler-30b. Each portion of the lightcurve is centered where the transit would be if it followed the best-fit linear ephemeris. Instead, we see that the timing of the planet varies by of order a day. The standard *Kepler* pipeline (Jenkins et al. 2010) assumes near-periodic transits, but the transits are deep enough for detection despite its strong acceleration. If the transits were considerably shallower, it may not have yielded a significant signal before the phase changed by more than a transit duration (García-Melendo & López-Morales 2011). To address this, the transit-timing subteam of *Kepler* is currently developing search algorithms that assume either a

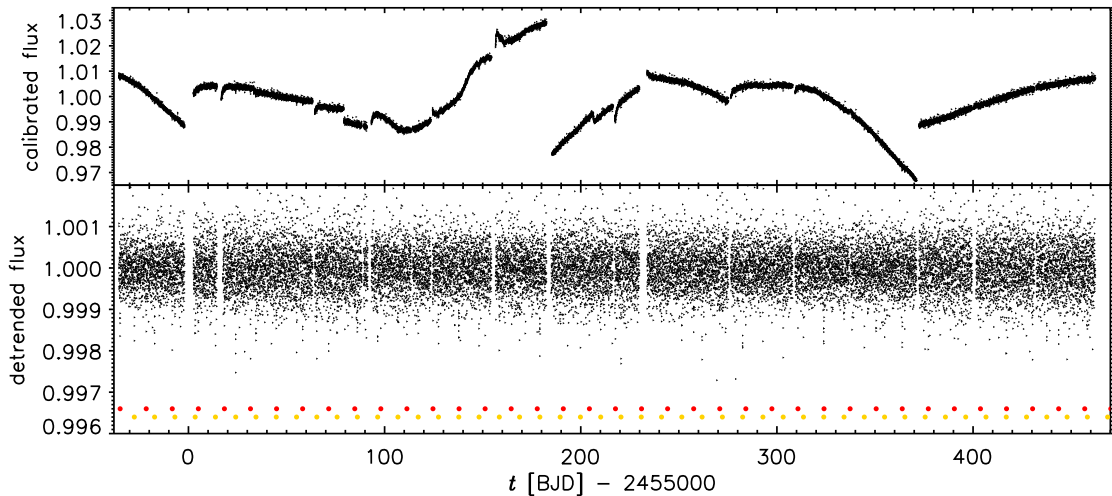


Figure 2. Kepler-29 lightcurves. *Upper panel:* the quarter-normalized, calibrated *Kepler* photometry (PA); *lower panel:* the detrended, normalized flux. The transit times of each planet are indicated by dots at the bottom of each panel.

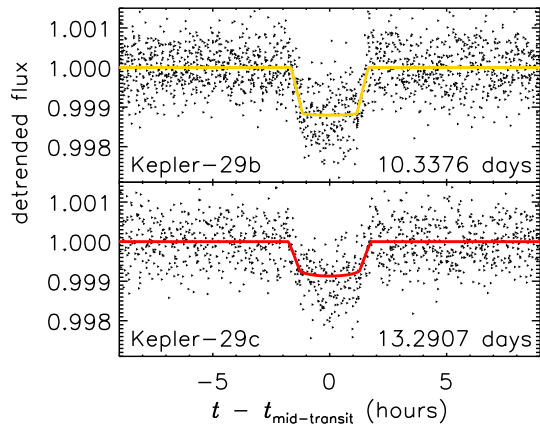


Figure 3. Kepler-29 phase curves based on detrended, normalized flux. Each transit is shifted to its measured midtime, and transits with midtimes within 5 hours of a different planet’s midtime are excluded from both this plot and from the model fits. Overplotted are transit models, box-car smoothed to the 29.4 minute cadence. The colors correspond to the dots of figure 2.

quadratic, a sinusoidal, or a non-specified quasi-periodic ephemeris.

Finally, consider Figure 11, the individual transits of Kepler-30c. The residuals (with a $3\times$ zoom) are shown beneath each transit. The average transit lightcurve does not capture some of the variations from transit-to-transit, at the level of $\sim 10\%$ of the planet’s depth. We suggest this is due to the planet transiting over starspots, which are clearly visible in the out-of-transit curve at the level of a few percent (fig. 6). To extract the spot period from the lightcurve, we used a slightly modified version of the Discrete Correlation Function of Edelson & Krolik (1988) (see also White & Peterson 1994), as was recently applied to the CoRoT-7 data (Queloz et al. 2009), and obtained $P_{\text{rot}} = 15.25 \pm 0.25$ days. Modeling the spot-crossing signal during transits may allow the measurement of the spin orientation of the host star rel-

ative to the planets’ orbits in this particularly valuable multiple-planet system (Sanchis-Ojeda et al. 2011; Nutzman et al. 2011; Désert et al. 2011). Kepler-30c (also known as KOI-806.02) was recently detected in transit from the ground, by Tingley et al. (2011), who made the point that it will serve as an interesting system to continue following even after *Kepler* finishes its mission.

3.1.3. KOI-935 = Kepler-31

Kepler-31 is a system of four planet candidates spaced just wide of a 1:2:4:8 resonant configuration. Its lightcurve is shown in Figure 12 and its phase curves in Figure 13. From the nominal models, only the middle two (Kepler-31b and Kepler-31c) are expected to show a > 1 min variation, big enough to be detected in *Kepler* data. The timescale due to this near-resonance is predicted as

$$P_{\text{ttv}} = 1/|2/42.6330d - 1/20.8609d| = 980d. \quad (3)$$

Thus, we have the now-familiar situation that a long-timescale variation is predicted due to the interaction. In this case we supplemented the dataset with quarters 7 and 8 as well, which were able to capture more of this long-timescale variation. The data for Kepler-31b indeed clearly show a variation matching the prediction (Fig. 14, top panels), with a low false alarm probability. We are seeing its orbital period increase due to the torque exerted by a 2:1 mean-motion resonance. The magnitude of this torque depends on both the planets’ masses and eccentricities, so it is not surprising the theory underpredicted the amplitude by a factor of ~ 3 . Thus we confirm that these two objects are interacting, which combined with the mass limits set in section 4.1, confirms them as planets.

The hint (FAP=3.4%) of TTVs of Kepler-31c due to Kepler-31b does not itself satisfy our statistical criterion. Nevertheless, the clear detection of TTVs in Kepler-31b consistent with the timescale predicted due to Kepler-31c provides evidence that they are in the same physical

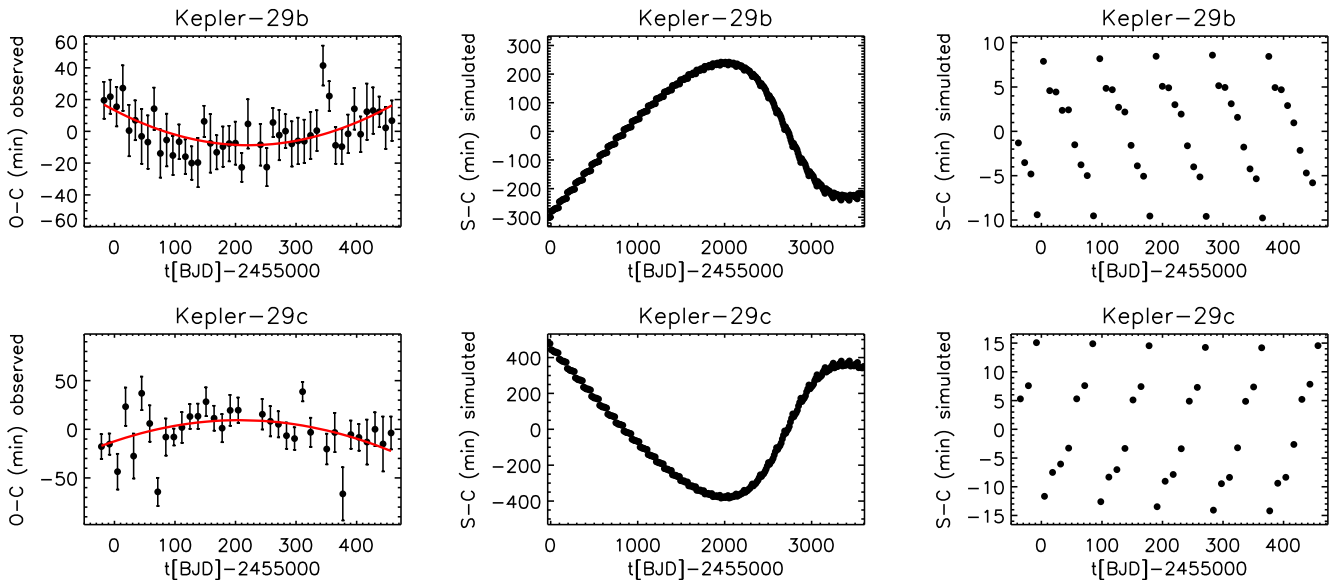


Figure 4. Timing diagrams of Kepler-29. In the left hand panels, the data are plotted. In red is the best-fitting sinusoid of the theoretically-determined dominant perturbation frequency. From the amplitude of this sinusoid we determine the significance of the TTV detection. In the middle panels a nominal model, in which the planets are presumed to start out on circular, coplanar orbits, shown for the decade-span on which we determine the dominant perturbation frequency. Although this is a poor fit to the data, it illustrates that a very long-timescale and large-amplitude variation is expected due to the planets’ orbits being right on top of a resonance with each other. Also, a very much smaller variation with a 93 day period is expected. In the right-hand panels, we have zoomed in on the first part of that signal; these variations are marginally detected in the data.

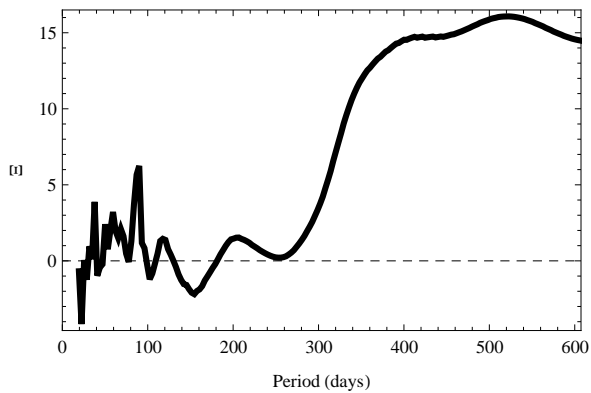


Figure 5. Cross-correlation statistic (paper III) as a function of TTV period for Kepler-29 b/c. The dominant variation is of long period (as in Figure 4), and a secondary and only marginally significant peak occurs at ~ 90 days.

system.

The system also has a long-period candidate KOI 935.03 and an inner candidate KOI 935.04, but these are not visibly interacting.

3.1.4. KOI-952 = Kepler-32

Kepler-32 boasts five planet candidates, one of the richest systems among the *Kepler* discoveries (Lissauer et al. 2011b). Its lightcurve and phase curves are plotted in Figures 15 and 16, respectively. The lightcurve has variations suggesting a starspot signal, in which case we determine $P_{\text{rot}} = 37.8 \pm 1.2$ days using an autocorrelation

technique as above.

Candidates .01 and .02 have short orbital periods and lie close to a 3:2 mean-motion resonance: $P_{.02}/P_{.01} = 1.483$. Therefore, we expect a short TTV timescale:

$$P_{\text{ttv}} = 1/|3/8.7522d - 2/5.9012d| = 260d. \quad (4)$$

The observed timescale of TTVs is consistent with this expectation from the nominal N-body integrations (Fig. 17). The amplitude is somewhat larger than predicted by the nominal model (~ 2.6 and $3.3 \times$). This is not unexpected as even modest eccentricities can significantly increase the amplitude and completely change the phase of the predicted TTVs. The amplitudes also scale with the planet masses, which could be larger than those adopted in our nominal model. The ratio of TTV amplitudes for Kepler-32b and Kepler-32c agrees with the predictions of the nominal model to $\sim 20\%$. Despite these uncertainties, the requirement of dynamical stability provides firm upper limits on the planet masses. Thus, we confirm this pair of planets and rename them as Kepler-32b and Kepler-32c.

Based on the nominal N-body integrations of the five planets, we expect shorter timescales and smaller amplitudes for transit variations of KOI-952.03, .04, and .05. Indeed, no significant transit time variations were seen in them, nor do they induce detectable variation in Kepler-32b or Kepler-32c, so we cannot confirm them via TTVs at this time.

3.2. Identification of the Host Star

In this section we discuss the probability that the planets are actually hosted by a star other than the target. The area on the sky in which that other star is allowed is

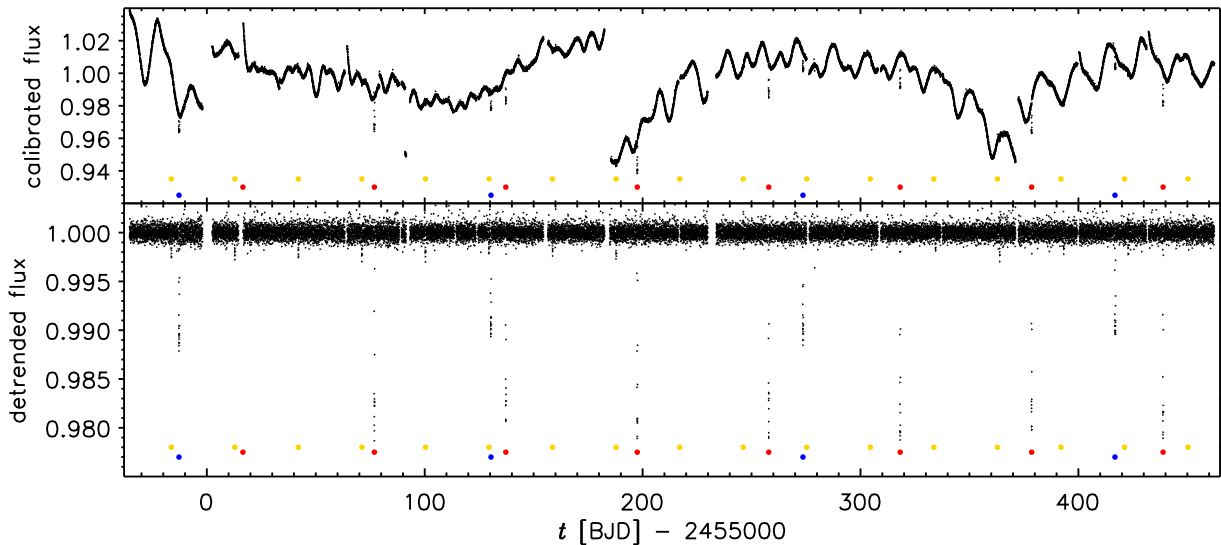


Figure 6. Kepler-30 / KOI-806 lightcurves. *Upper panel:* quarter-normalized calibrated lightcurves; the stellar rotation period of 15.25 ± 0.25 days is manifested as out-of-transit variations caused by spots. *Bottom panel:* Detrended, normalized flux. The transit times of each planet are indicated by dots at the bottom of each panel.

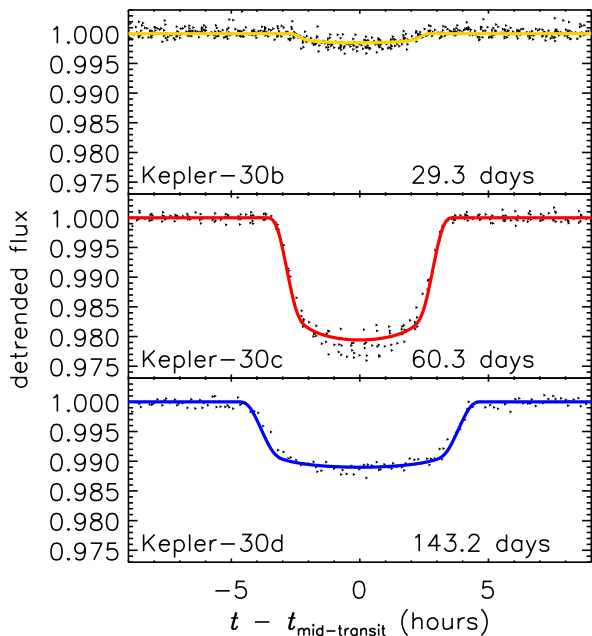


Figure 7. Kepler-30 / KOI-806 phase curves, in the style of figure 3.

limited via lack of movement of the centroid during transits (Torres et al. 2011, Bryson et al. in prep). Because of the low space density of transiting planetary systems, it is generally rather unlikely (quantified for each candidate below) that it is hosted by an unrelated background or foreground star, which is a minority contribution to the light of the target. In comparison, because most stars are components of binaries, it is not inconceivable that our targets are physically bound binary stars where the second component is not detected, and the fainter com-

ponent hosts the interacting planets (probability quantified below). To pursue these calculations, we assume a maximum planetary radius consisting of the upper envelope of the mass-radius relation of known exoplanets. If the radii implied by a blend scenario are either above that limit or imply masses too large for dynamical stability given the configuration of planets, then we reject that blend scenario. Now we discuss details of each system.

3.2.1. Kepler-29

Kepler-29 has low contamination from surrounding stars. The nearest stars to Kepler-29, listed in the *Kepler* Input Catalog (KIC), are KID 10358756, a $Kp = 17.5$ mag star located 6.5 arcsec to the south, and KID 10358742 located 9 arcsec away. We examined the UKIRT J-band image and obtained a new image from Faulkes Telescope North in the Sloan-r band (figure 18); neither showed evidence of additional companions to a magnitude difference of ~ 5 in to ~ 1 arcsec. We therefore adopt the aperture contamination calculated using stars in the KIC alone.

The planets pass the centroid test: the photocenter out-of-transit and during transit are consistent to within $(2\sigma, 1\sigma)$ for planets $(.01, .02)$ respectively. This rules out out background stars as the planet host if they are further than $Rc = (0.7, 0.8)$ arcsec from the target, where Rc is the $3\text{-}\sigma$ radius of confusion. Thus none of the background stars in the image can be the host. Next we computed the space density of background stars, to determine the chance that the planetary system is actually around a star other than the target. That is, we assume that the TTV signature robustly indicates this system is planetary, but we wish to see the probability it is around a star other than the one we have characterized.

Stability limits (section 4.1) require that the planets cannot be too massive relative to their host, otherwise they would be unstable. In this case, the mass ratio of both planets to their host must be $\lesssim 2 \times 10^{-4}$. With

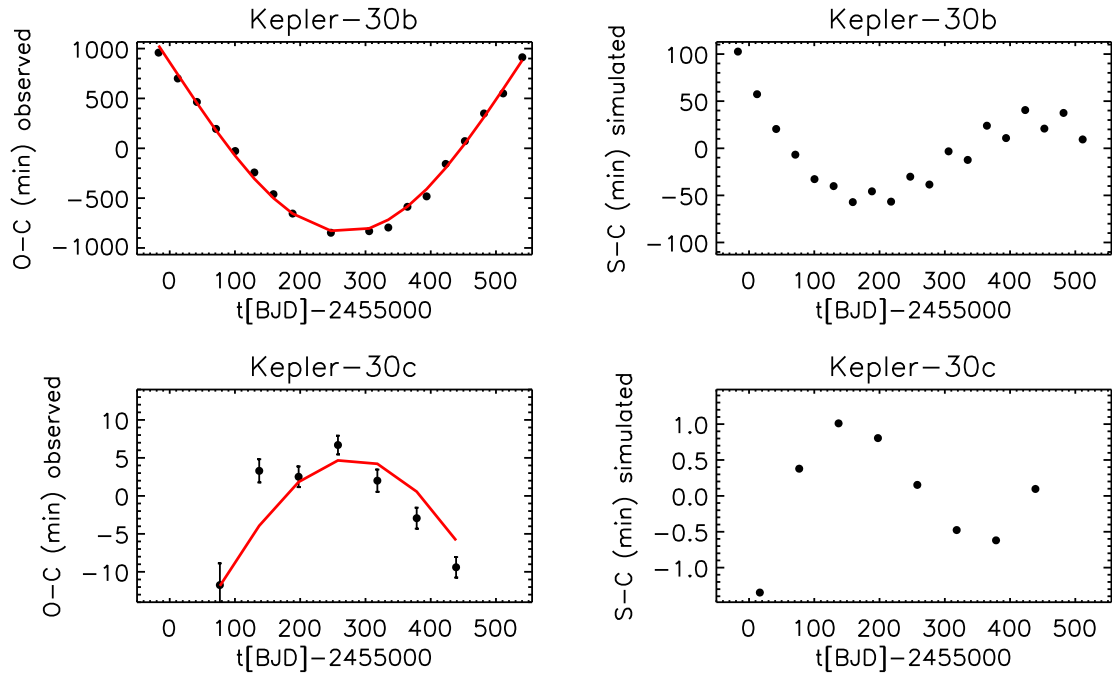


Figure 8. Kepler-30. Transit timing diagram with theoretical model compared, for the interaction between Kepler-30b and Kepler-30c. Panels are the same as in Figure 4.

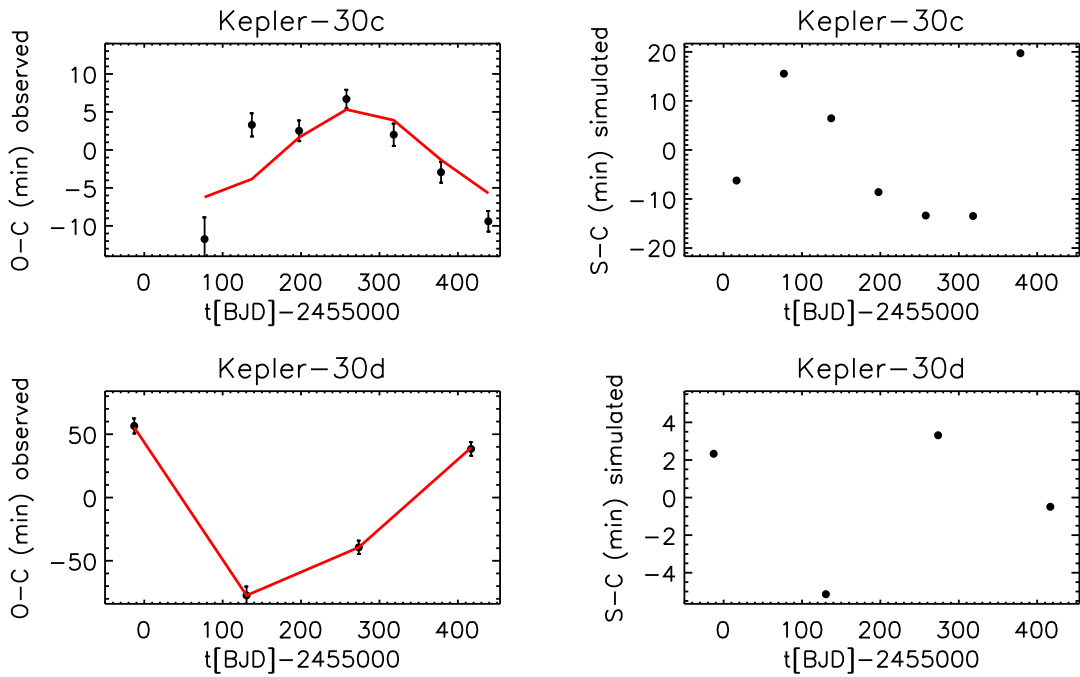


Figure 9. Kepler-30. Transit timing diagram with theoretical model compared, for the interaction between Kepler-30c (top) and Kepler-30d (bottom). (Ignore the labels above the plots for now, as they will be finalized with a Kepler number; these plots are for c and d.) Panels are the same as in Figure 4.

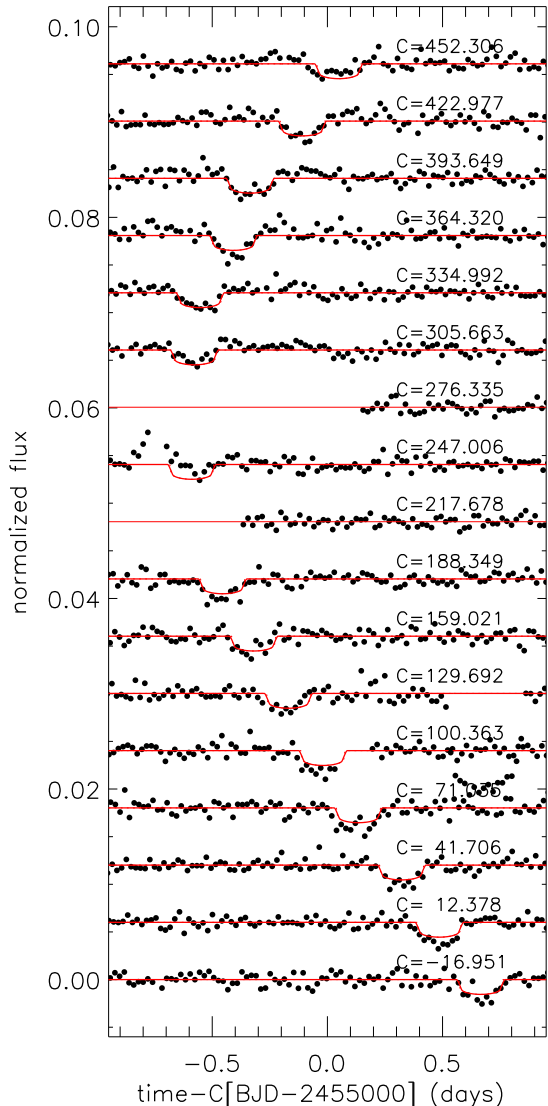


Figure 10. Individual transits of Kepler-30b. Each portion of the lightcurve is shown with its transit shifted to the best linear-ephemeris value, and the model is shown with the best-fit transit time taken into account. This is the biggest transit timing variation yet reported in multiple-planet systems.

such low masses, we consider $1R_{\text{Jup}}$ to be a robust upper limit for the radii of the planets. This sets the constraint on the maximum magnitude difference that the blending star can have. Any star fainter than this limit would not contribute enough to the combined flux to generate an eclipse as deep as observed (830 ppm). Based on the U-shaped light-curve, we assumed that grazing transits were excluded, such that $(R_p/R_*)^2$ is a good approximation of the (undiluted) depth. We used Yonsei-Yale isochrones (3 Gyr, solar metallicity) to relate the maximum allowed magnitude difference (ΔK_p) to the spectral type and mass of the blending object.

The background host hypothesis splits into two distinct cases: the planets are larger and (1) orbit a physically unassociated star, or (2) orbit an unseen binary companion of the target.

For the former, we used the Besancon model of the

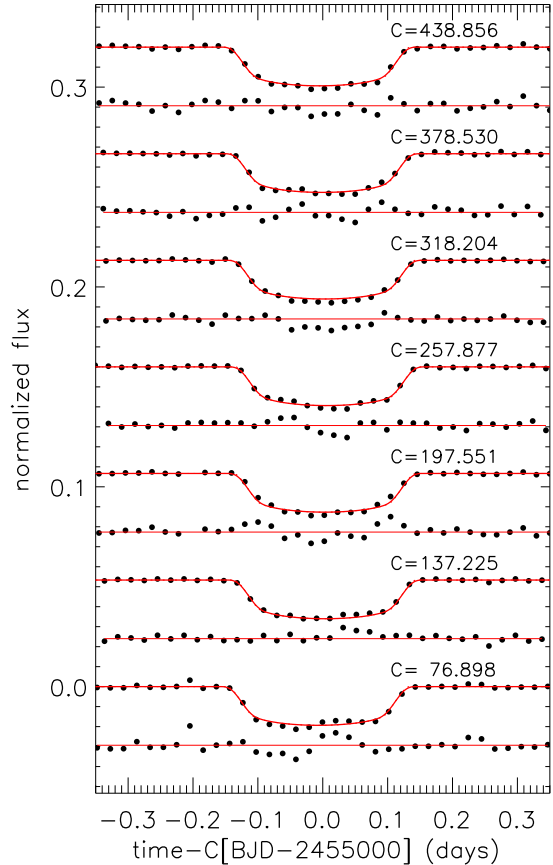


Figure 11. Individual transits of Kepler-30c (KOI-806.02, the planet observed by Tingley et al. 2011), in the style of figure 10. Below each transit is shown the residuals from the model, scaled up by a factor of 3 to better show the deviations. The largest variations appear in eclipse and are correlated point-to-point. Large starspots are visible in the lightcurve; we hypothesize this excess variability comes from the planet transiting over them.

galaxy (Robin et al. 2003) to estimate the number of background stars within the region allowed by the centroid shift result *and* the region in the allowed magnitude difference (or stellar mass). The probability of having a background star in this region is 0.6%. If we assume (conservatively) that the more massive planets on the background star are as likely, a priori, as less massive planets on the target star, then the odds ratio that the target star hosts the planets rather than a background star is $\sim 170 : 1$.

Next we calculate the probability of the latter case, that the planetary system is orbiting an unseen stellar companion to the target star. The blends involving stars less massive than a $0.6M_{\odot}$ star would need large planets, which in the range of known exoplanets would be too massive to be stable. In the range $0.6\text{--}0.8M_{\odot}$, we can use the (Sloan) $r - (2 \text{ MASS}) K$ color of the target to rule out such blends, as they would not correspond to the observed color. A blended star more massive than $0.8M_{\odot}$ is allowed, and we call this scenario a ‘twin star’ blend. It is possible to put limits on such blends because we do not see two stars in the images, nor do we see two sets of lines in the spectrum. The only remaining

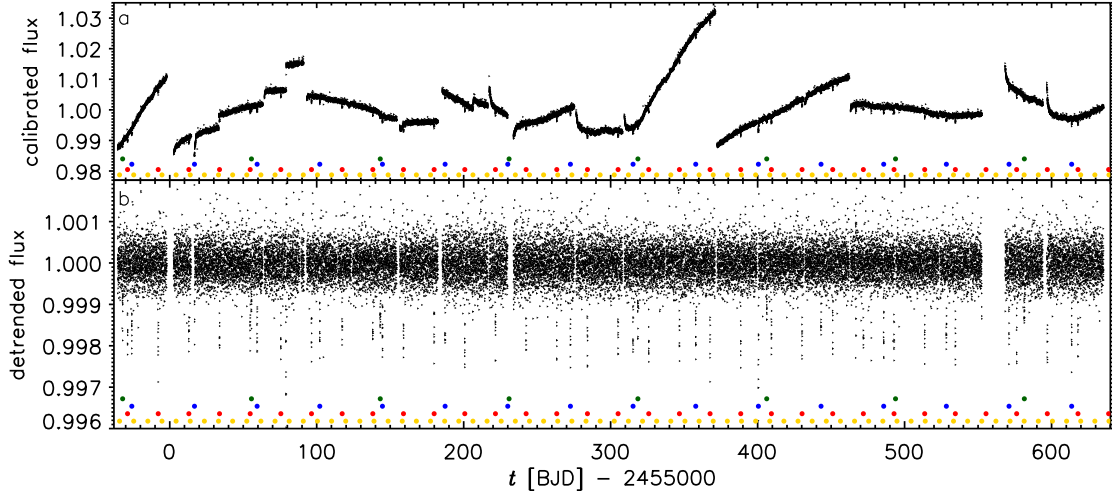


Figure 12. Kepler-31 lightcurves, in the style of figure 2.

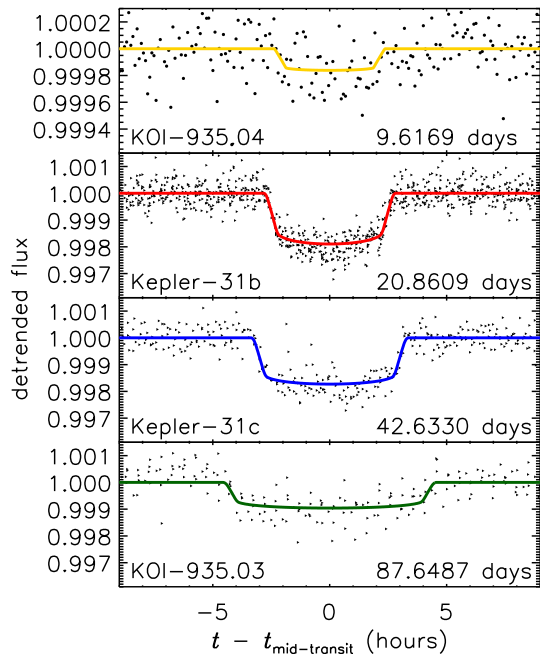


Figure 13. Kepler-31 phase curves, in the style of figure 3. For the small inner candidate KOI-935.04, the phase is with respect to a linear ephemeris, the data in that panel are binned together in phase. The vertical scale of that panel is 20% of the other panels.

case is that the two twins have a large separation along the line of sight (a small velocity difference) but not in the plane of the sky. If there were such a case, it would correspond to twice the light, so the undiluted depth of transits would be twice as large, so the planets would be $\sim \sqrt{2}$ larger.

Even without employing that constraint, we use Raghavan et al. (2010); Duquennoy & Mayor (1991) to determine the distribution (frequency/mass ratio) of binaries and find the probability of having an unseen companion star in the allowed mass range ($0.8\text{-}1.0M_{\odot}$) is 7%.

For this target, which has a clean centroid and closely-packed planets that would go unstable if they were gas-giant masses, we find that background hosts are much less likely than the target star being the host.

3.2.2. Kepler-30

We obtained an I-band image of Kepler-30 from Lick 1-m telescope, and found no stars besides those in the KIC, the closest of which is $Kp = 19.8$ mag KIC 3832477, 7.6 arcsec to the ENE. A star ~ 3 arcsec to the E is marginally detected in J-band with UKIRT, suggesting it is $\gtrsim 5$ magnitudes fainter than the target in Kp. It cannot host the 2% deep transit of Kepler-32c, and we neglect its additional contribution to the dilution. Furthermore, since planets c and d produce deep transits, their centroid information is particularly valuable. Their transits have a consistent centroid with the target to $\sim 1\sigma$ in either case, and they limit the distance of a putative blend hosting the system to be within $R_c = 0.2$ arcsec of the target.

As a routine part of vetting planet candidates, the depth for odd numbered transits was compared to the depth for even numbered transits. For the other candidates reported in this paper, there is agreement to $\sim 3\sigma$; however in this system, they disagree by 16σ for c and 4σ for d. In some cases, that would point to a near-twin blended eclipsing binary causing the events. In this case, we have already identified via figure 11 that transiting over starspots is the probable cause of these depth variations.

Using the same procedure as for Kepler-29, we find the probability that an unassociated background star hosts the planets is $\sim 2 \times 10^{-4}$. In this case, a physical binary companion cannot host the planets, as then their depths would be large despite dilution, and their inferred radii would be larger than any planetary radii thus far measured.

3.2.3. Kepler-31

Kepler-31 has low contamination from surrounding stars; no stars are seen within 8 arcsec in a UKIRT J-band image, and the closest comparably bright star is

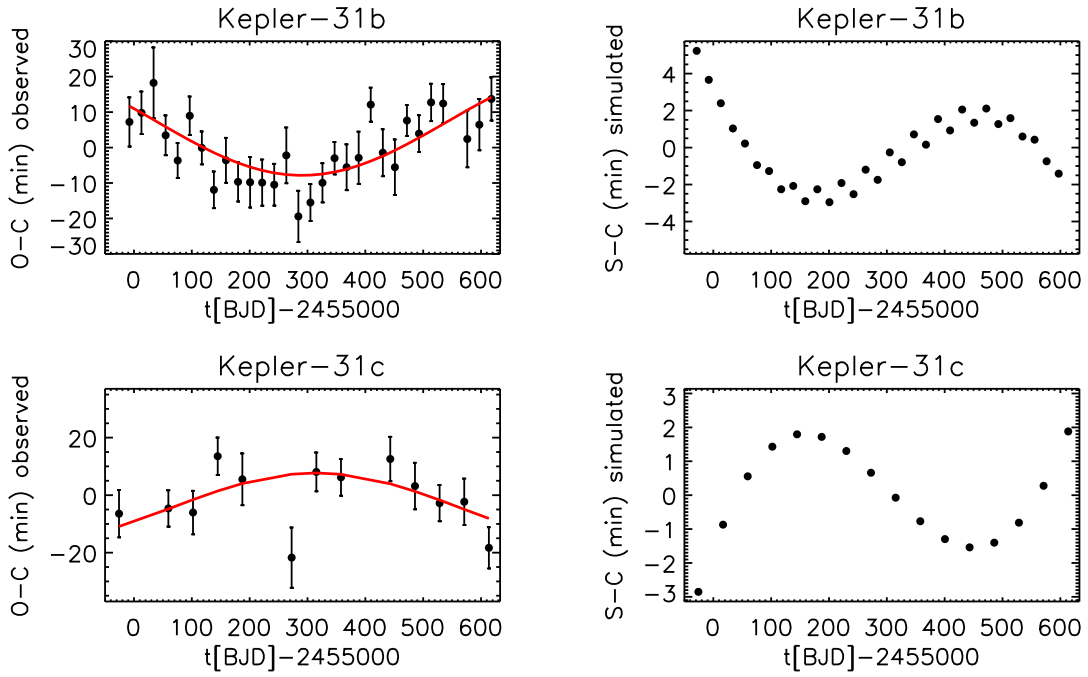


Figure 14. Kepler-31. Transit timing diagram with theoretical model compared. The data for planets b and c show curvature on a long timescale, as predicted by a theoretical model in which they torque each other due to the close 2:1 resonance.

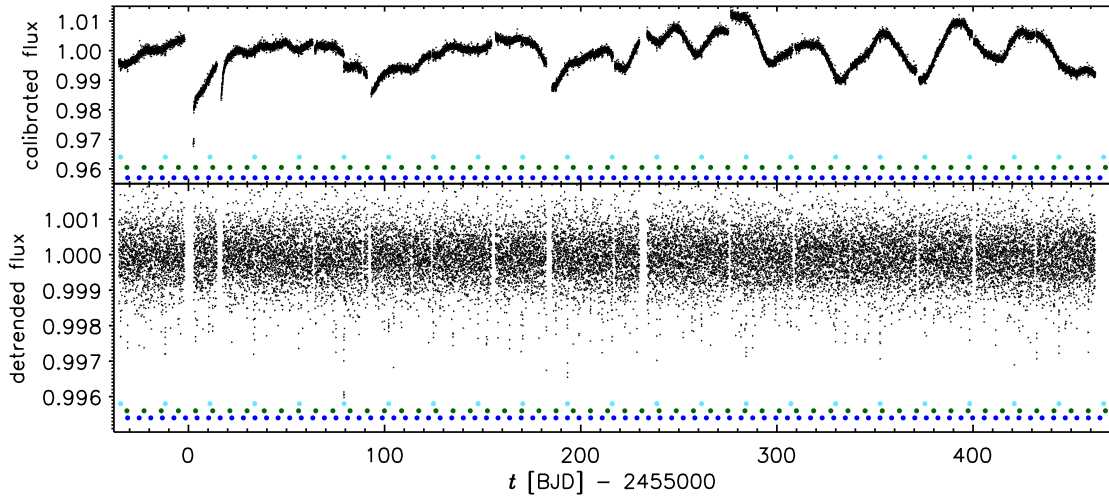


Figure 15. Kepler-32 lightcurve. *Upper panel:* quarter-normalized calibrated lightcurves; the stellar rotation period of 37.8 ± 1.2 days is evident in quarters 5 and 6. *Bottom panel:* The bottom, middle and top rows of dots (blue, green, teal) are for Kepler-32b, Kepler-32c and KOI-952.03. (The short-period candidates KOI-952.04 and KOI-952.05 are not detected in individual transits, so no pointers are given for them.)

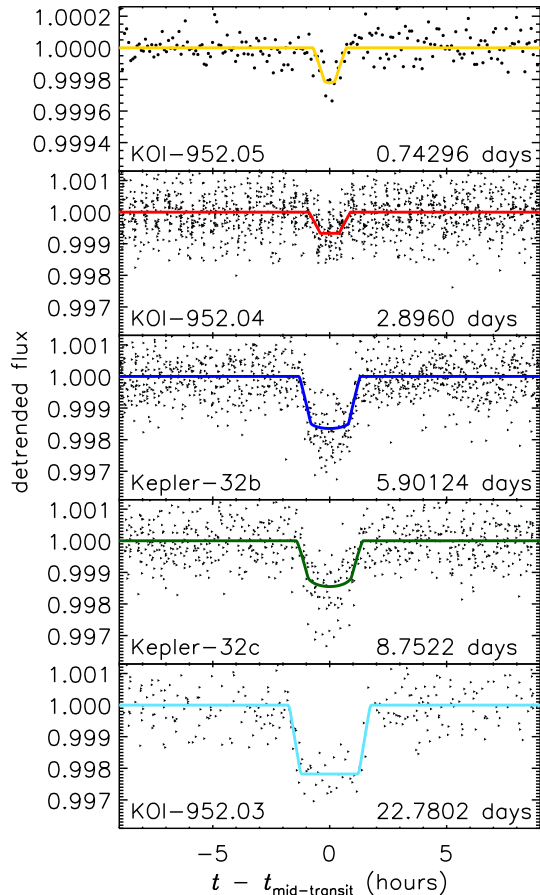


Figure 16. Kepler-31 phase curves, in the style of figure 3. For the small inner candidate KOI-952.05, the phase is with respect to a linear ephemeris, the data in that panel are binned together in phase. The vertical scale of that panel is 20% of the other panels.

KIC 9347893, 9.4 arcsec to the west. Moreover, the centroid information has all transits coincident within 1σ of the target. The transits cannot be hosted by a background star further than $R_c = (0.3, 0.5, 0.8)$ arcsec in the case of Kepler-31b, Kepler-31c, KOI-935.03 respectively. For KOI-935.04, the transits are too shallow for a constraining centroid analysis.

Again pursuing probability calculations as above, the chance of a star unassociated with the target being the actual host is only $\sim 3 \times 10^{-4}$. The probability of a physical companion hosting the planets is ~ 0.04 .

3.2.4. Kepler-32

A J-band image from UKIRT shows the nearest star to be KID 9787232, $\sim 6.6''$ to the west, resulting in rather low contamination.

The centroids during transit for Kepler-32b and Kepler-32c differ from those out-of-transit by only $\sim 2\sigma$, roughly consistent with measurement uncertainties. The $\sim 3\sigma$ radii of confusion R_c are $0.5''$ for Kepler-32b and $0.8''$ for Kepler-32c. For KOI-952.03, .04, and .05, the transits are too shallow for a constraining centroid analysis.

The host star is an M-dwarf and therefore of special in-

terest. The Kepler Follow-up Program has obtained two spectra of Kepler-32: one spectrum from McDonald Observatory and one from Keck Observatory. Both spectra are weak due to the faintness of the star ($K_p=15.8$). The cross correlation function between the observed spectra and available models is maximized for temperatures of ~ 3900 K and ~ 3600 K, respectively. However, the atmospheric parameters are not well determined, as the star is cooler than the library of atmosphere models available. Both spectra are consistent with the KIC classification as a cool dwarf ($T_{\text{eff}} = 3911$, $\log g = 4.64$, $[M/H]=0.172$). We conservatively adopt these values of T_{eff} and $\log g$ with uncertainties of 200K and 0.3 dex and a $[M/H]$ of 0 ± 0.4 based on the KIC (Brown et al. 2011). By comparing to the Yonsei-Yale isochrones, we derive values for the stellar mass ($0.58 \pm 0.05 M_{\odot}$) and radius ($0.53 \pm 0.04 R_{\odot}$) that are slightly larger than those from the KIC. We estimate a luminosity of $0.06 \pm 0.02 L_{\odot}$ and an age of ≤ 9 Gyr.

Muirhead et al. (2011) have also obtained high-resolution IR spectrum of Kepler-32=KOI-952, finding a stellar $T_{\text{eff}} = 3726^{+73}_{-67}$, $[Fe/H] = 0.04^{+0.08}_{-0.10}$. Interpreting their data via Padova models (Girardi et al. 2002), they inferred a considerably less massive and smaller star. We encourage further detailed analyses of the host star properties, as these have considerable uncertainties that directly affect the sizes and masses for the planets.

The probability of a star unassociated with the target being the actual host is only $\sim 3 \times 10^{-3}$. The probability of a physical companion hosting the planets is ~ 0.34 . This latter number is relatively large in this case because all the transit depths are small, so they could in principle be much larger planets hosted by a star which is dramatically diluted. This opens up the possibilities for a very large range of companions (down to masses as low as $\sim 0.1 M_{\odot}$) that could host one or more of these objects, as long as transits near apocenter are invoked to match the durations (fig. 1).

4. PLANETARY MASS LIMITS

4.1. Dynamical Stability Analysis

Many of the systems in this paper and its companions (Papers II and III) are not completely solvable with present data; e.g., the gravitational interactions of the component planets do not yield unique solutions for their masses. Rather, there exists degeneracy between the masses and eccentricities, as was the case for Kepler-9 before radial velocity constraints were applied (Holman et al. 2010). However, we constrain them to be in the planetary regime because the pairs of planets all have small period ratios. In two-planet systems, a sharp boundary exists between provably stable orbits (Marchal & Bozis 1982) and orbits that are allowed to cross, according to energy and angular momentum conservation. This boundary is when the separation of the planetary semi-major axes, $a_{\text{out}} - a_{\text{in}}$, exceeds a certain number ($2\sqrt{3} \approx 3.46$, for coplanar, circular orbits) of mutual Hill spheres,

$$r_H = \frac{a_{\text{in}} + a_{\text{out}}}{2} \left(\frac{M_{\text{in}} + M_{\text{out}}}{3M_{\star}} \right)^{1/3}. \quad (5)$$

When the separation is only slightly closer than this, numerical integrations generally show the planets chaoti-

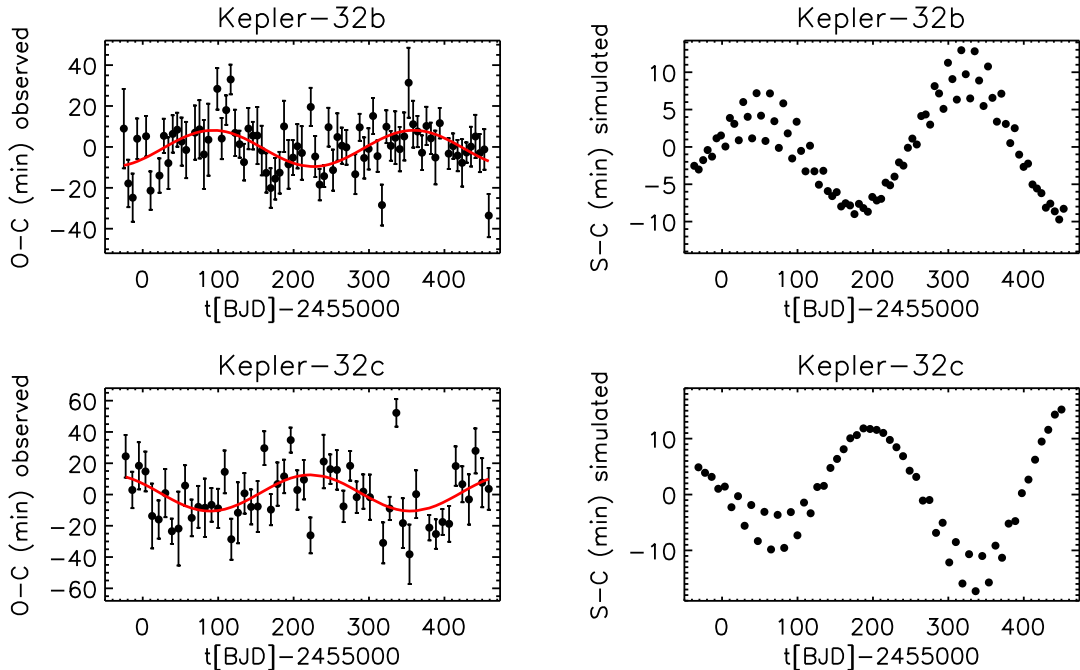


Figure 17. Comparison of measured transit times (left) and transit times predicted by the nominal model (right) for a system containing only Kepler-32b (top) and Kepler-32c (bottom). Details are described in the caption to Fig. 4.

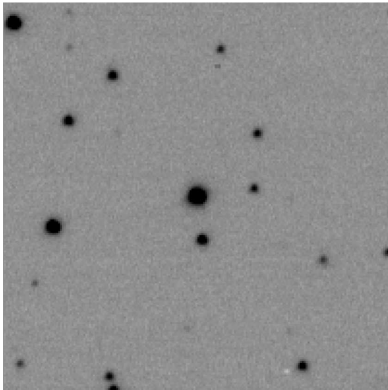


Figure 18. FTN optical (Sloan r) image of Kepler-29. The scale is 1 arcmin on each side, and north is up.

cally interact and have close encounters after only several million orbits, an astrophysically short amount of time (Gladman 1993; Barnes & Greenberg 2006). An exception is that planets locked in mean motion resonances may avoid each other due to the correlated phases of their orbits; Neptune and Pluto are a familiar example (Cohen & Hubbard 1965).

We ran a suite of numerical integrations for each planetary pair with a significant TTV interaction to determine when the masses would be too large to yield a long-term stable system. We used the HYBRID integrator within the *Mercury* package (Chambers 1999). Since we stopped after close encounters, the mixed-variable symplectic algorithm was exclusively used (Wisdom & Holman 1991), with a timestep $1/20$ th of the inner planet’s orbital period. An implementation of general relativistic precession was included

(Nobili & Roxburgh 1986; Lissauer et al. 2011b). We picked the planets’ ratio of masses from their ratio of radii according to the relation $M_{in}/M_{out} = (R_{in}/R_{out})^{2.06}$ (Lissauer et al. 2011b). We performed 6 integrations with differing total mass, starting at the theoretical stability boundary and becoming more massive by logarithmic steps of 0.25 dex. The orbits were taken as initially circular and coplanar, with phases determined from the *Kepler* data.

We stopped the integration when planets came within $3 r_H$ of each other, calling this time the instability timescale. We ran only one integration at each mass, so we recognize that this investigation only identifies the order of magnitude of that timescale – however, consistent with previous investigators (Chambers et al. 1996; Duncan & Lissauer 1997) we find that a factor-of-two change in mass causes many orders of magnitude of difference in instability time. Figure 19 gives the instability timescales as a function of planetary mass. We determine the mass upper limits based on the minimum mass for which the integrations start going unstable on $\lesssim 10$ Myr timescales; for this purpose, we do not need to run the integrations for the likely lifetimes of these systems. These limits are given in Table 3. These are quite conservative upper limits, and the true masses could all be quite smaller. Full modeling of the systems, including eccentricities, is required for a true mass measurement via transit timing variations (e.g. Kepler-11 by Lissauer et al.). Nevertheless, this exercise shows that all of the systems we are presenting should be considered “planetary” systems, rather than stellar systems.

In this investigation, we have simulated only pairs of planets and neglected additional planets, either other

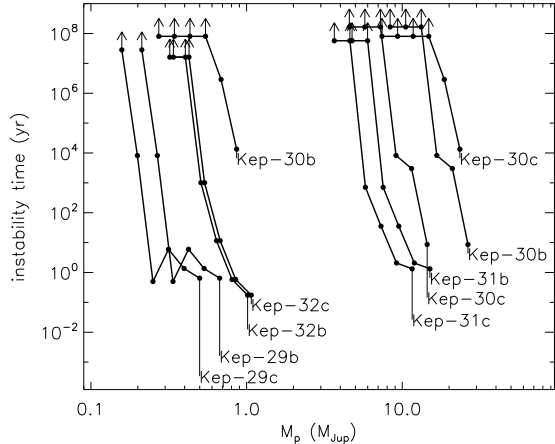


Figure 19. The time until instability, as a function of planetary mass. This figure shows that for these objects to be stable, they must have masses traditionally associated with the planetary domain.

transiting candidates or completely unknown planets. When third planets are added, stability constraints have been found by numerical integrations to become even more stringent (Chambers et al. 1996; Chatterjee et al. 2008; Fabrycky & Murray-Clay 2010a). An interesting exception was discussed by Raymond & Barnes 2005, but the third planet in that case quenched secular eccentricity cycles, which is not the chaotic mechanism for instability we have investigated above. Therefore the future confirmation or discovery of such planets will not compromise the conclusions here.

Similarly, we neglected possible eccentricity in the planets. For non-resonant cases, non-zero eccentricities would only serve to bring the planets closer together at conjunctions, making them more unstable (Duncan et al. 1989; Zhou et al. 2007). However, eccentricities can actually increase the stability of resonant pairs. This effect could prolong the lifetime of Kepler-29, such that its true upper-limit masses are underestimated by at least a factor of several. Since these orbits are closely packed however, resonances besides the 9:7 can overlap with it, leading to chaotic instabilities. Using the $\Delta a/a > 1.3\mu^{2/7}$ criterion for stability (Wisdom 1980), the maximum planet-to-star mass ratio is $\mu = 0.02$. If that mass is shared among the planets, then they both fall in the planetary regime ($\lesssim 10M_{\text{Jup}}$).

4.2. Preliminary Dynamical Fits to the Transits Times

We have used the method first developed for the Kepler-9 and Kepler-11 discovery papers (Holman et al. 2010; Lissauer et al. 2011a) to fit preliminary dynamical models to all the planetary pairs of this paper and the two companion papers.

Using the Levenberg-Marquardt algorithm to drive 3-body numerical integrations, minimizing the χ^2 of the residuals of the data minus the model. The free parameters are the mass M_p of each planet and the Jacobian coordinates at dynamical epoch BJD 2455220.0 of each planet: orbital period P , epoch of mid-transit T_0 , and the in-sky-plane and perpendicular-to-sky-plane components of the eccentricity vector, $e \cos \omega$ and $e \sin \omega$, respectively. We ignore the dynamical effect of any plan-

ets that remain candidates in this work, just focusing on the interaction between the planets that show significant TTVs.

The resulting fit parameters may be found in Table 5. In many cases, the eccentricities and masses are very highly correlated, resulting in poor errors on each quantity. However, we report many more decimal places beyond what seems significant, as to make these fits reproducible by others. We note the contribution to χ^2 for each planet and the number of degrees of freedom (d.o.f.) for that planet, meaning its number of data points minus the 5 free parameters used to model it. (In two-planet fits, there were 10 free parameters total.) In fits that are statistically acceptable, χ^2 should equal d.o.f. to within a few times $\sqrt{\text{d.o.f.}}$. Of the systems confirmed in this paper, the poorest fit was for Kepler-30 / KOI-806, which might be attributable to starspots' effect on estimates of transit times.

We found that Kepler-29, the system at the 9:7 resonance, needed special treatment. Allowed to fit freely, the eccentricities solved for large values, causing the planets to cross. Because of phase protection by the resonance, this was allowed by the data, but after a secular timescale the planets began chaotic scattering. Therefore in the fit reported in Table 5, we restricted the absolute value of each eccentricity components to be less than 0.05. The result was integrated using the Bulirsch-Stoer algorithm in *Mercury* (Chambers 1999) for 1 Myr, during which it showed stable and regular orbital oscillations. In other systems the eccentricities are quite moderate compared with the separation in semi-major axis, and we have not verified stability for these. In future detailed fits to the data, stability could be used as a principle guiding the results.

In only a few cases are the masses meaningfully measured, according to the formal error bars (e.g. $\gtrsim 3\sigma$). These error bars sample only the local minimum of the fit. We recognize that drawing meaning from the local curvature about the entire probability surface is hazardous. However, we hope this preliminary work on transit fits will inspire other investigators to exhaustively explore orbital configurations that fit the data. In the meantime, we tried to set 3σ upper limits on the masses of the planets via the method developed in Holman et al. (2010): we moved the mass of one of the planets away from the best-fit, incrementing by $\sim 50\%$, and solving for the other parameters each time. When χ^2 had grown to 9 greater than the χ^2 of the best-fit, we used the mass of the planet in that fit to define the 3σ upper limit. These limits are reported in table 5. In comparison to the stability study, these TTV limits on mass are much tighter. However, this method is rather delicate, in that we have not fully explored the global parameter space for a possibly more massive planet. The stability study provides more robust mass upper limits on the masses of these planets.

5. DISCUSSION

Taking stock of the results, we have

- developed a new approach to confirming planets, by testing whether the transit timing signal is consistent with that produced by a known perturber, a second transiting planet,

- applied this approach to *Kepler* transit timing data, and confirmed 9 planets in 4 planetary systems (and reconfirmed 16 planets in 8 additional systems),
- showed that their masses must be in the planetary regime via stability arguments, and provided dynamical fits to the data.

The systems discussed herein have remarkable properties.

Kepler-29 is clearly engaged in a second-order resonance, which has only been observed for the 3:1 resonance previously (HD 60532; Desort et al. 2008; Laskar & Correia 2009). In such cases, adiabatic capture from low-eccentricity is possible, but at a finite speed of migration, the capture probability is enhanced if planets migrated towards each other on eccentric orbits (Rein & Papaloizou 2010; Mustill & Wyatt 2011). Previously for systems of super-Earths, theorists (Terquem & Papaloizou 2007; McNeil & Nelson 2010; Ida & Lin 2010; Liu et al. 2011; Pierens et al. 2011) have suggested planets could be about this close to one another and trapped in resonances, but they have always focused on first-order resonances. Within the context of those formation models, the relative proportion of higher order resonances is now a pertinent question.

Kepler-30 is perhaps the most dramatic system described here, having properties similar to multiple planet systems long-known from Doppler surveys. The inner planet b has a > 1 day swing in its transit times, perturbed by its near-2:1 outer companion, c. This situation is very similar to that predicted by Agol et al. (2005) for the 2:1-resonant pair GJ 876 b/c, as the outer two planets clearly have gas-giant size. Continued monitoring of the transits may be able to give unique parameters for this system, and future information about duration variations or lack thereof may allow a measurement of their mutual orbital inclination. Planet c has a clear spot-crossing signal; its depth varies as a function of the spot phase of its host star. With careful spot modeling, this may allow the interpretation of the orientation of the host star’s spin relative to the planets’ orbits. Moreover, its transits are rather deep, from which we infer a large radius (Table 3: $1.34 \pm 0.15 R_{\text{Jup}}$). This is larger than expected for a planet receiving so little irradiation: the theoretical models by Fortney et al. (2007) are no bigger than $\sim 1.2 R_{\text{Jup}}$, and Demory & Seager (2011) confirmed that observationally using *Kepler* giant-planet candidates. We entertained the notion that this increased depth might be due to rings (Schlichting & Chang 2011), but unfortunately the characteristic “shoulders” were not seen in the transit lightcurve.

Kepler-31 has a 20.9-day planet and a 42.6-day planet now confirmed. Two other candidates, at 9 and 88 days, are present yet remain unconfirmed. If they can be confirmed at a later date, this system will be in an extraordinary near-1:2:4:8 resonant chain. Evidence for that sort of architecture has been building on several different fronts: radial velocity detections (HD 40307: Mayor et al. 2009; GJ 876: Rivera et al. 2010; HD 20794: Pepe et al. 2011), and a dramatic 4-planet system discovered by direct imaging (HR 8799: Fabrycky & Murray-Clay 2010b; Marois et al.

2010). It has even been suggested that the Solar System giant planets began in a multi-resonant configuration (Morbidelli et al. 2007; Thommes et al. 2008), albeit with links more compact than 2:1 resonances (Masset & Snellgrove 2001; Pierens & Nelson 2008).

Kepler-32 is a particularly clean case of anticorrelated transit times that also have a timescale matching baseline expectations. It is particularly interesting to confirm these planets, because their host star is an M-dwarf, around which small planets appear to be particularly abundant (Howard et al. 2011). The lightcurve boasts 3 additional candidate planets as well, making a particularly rich system.

We can attribute most of these signals to a slight displacement of the planets’ mean motions from a strict commensurability: they are involved in a “great inequality,” the orbital element oscillations of Jupiter and Saturn due to their displacement from the 5:2 resonance. The same sort of perturbations are detected in the system of planets orbiting PSR1257+12 (Rasio et al. 1992; Malhotra et al. 1992; Peale 1993; Wolszczan 1994). The planets torque each other’s orbits, resulting in a period increase or decrease, depending on where the location of conjunctions is relative to their periapses and to the line-of-sight. The departure from commensurability causes this location to move, generating a predictable fluctuation in their orbital periods. The timescale for this fluctuation is easily calculated from their orbital periods: equations 1-4. A general feature is that large-amplitude timing signals take many orbits to manifest themselves. If the *Kepler* mission is extended to eight years, this method would reach its full potential for planetary pairs with longer “great inequality” or libration timescales (e.g., Kepler-29, fig. 4). As the *Kepler* mission seeks to confirm longer-period candidates, in particular candidates in the habitable zone, we will be attempting transit timing analyses based on fewer transits. Dynamical theory may be required to condition our expectations about transit timing variations. This paper is a stepping stone to that type of analysis.

Along with Papers II and Paper III, we have confirmed 21 planets in 10 systems. The transit timing method has very little bias with respect to the magnitude of the stellar host, as planetary systems with large, detectable perturbations are hosted by stars throughout the sample. This contrasts with other *Kepler* confirmations so far, which have mostly relied on ground-based (and *Spitzer Space Telescope*) follow-up to confirm the planetary nature of the transiting objects. In particular, we show in Figure 20 that the current TTV confirmations are drawn from a very much fainter population than the previous confirmations.

In two of these systems, as well as systems in Papers II and III, additional candidate planets have been found, but not confirmed via TTV or other methods. *A priori*, it has been argued that planet candidates in multiple-planet systems have a higher fidelity than planet candidates that are by themselves, even before performing follow-up observations or analysis (Lissauer et al. 2011b; Latham et al. 2011, Lissauer et al. in press). Previously our team has pursued further analysis to validate additional small planets in TTV-active planetary systems: Kepler-9d (Torres et al. 2011), Kepler-10c (Fressin et al. 2011), and Kepler-18b (Cochran et al. 2011). For the

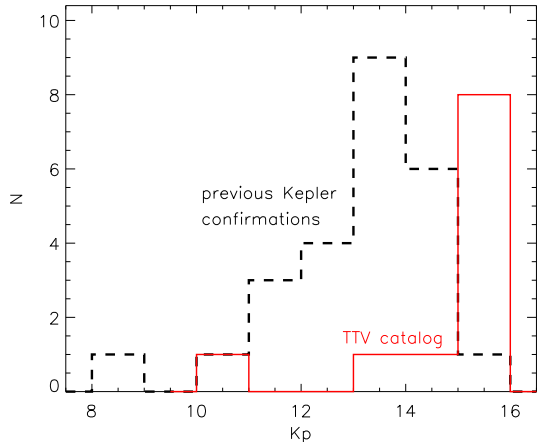


Figure 20. Histogram of stellar magnitudes in the *Kepler* band (K_p). The TTV catalog of planets confirmed by their interaction with each other (the 10 planetary systems from Paper II, Paper III, and this paper) is not dependent on follow-up with other telescopes, so it more uniformly samples the intrinsic magnitude distribution of *Kepler* stars. The previously confirmed planets, by the *Kepler* team (Kepler-4-Kepler-22) and also by Santerne et al. (2011b,a); Bouchy et al. (2011); Bonomo et al. (2011); Johnson et al. (2011), do depend on other telescopes, and thus tend towards brighter targets.

candidates listed here, many have good limits on R_c , the distance to which an unseen blend is a possible source of these transits. Their phased lightcurves are easily fit by planetary lightcurves (“U” shaped) rather than preferring blended binary lightcurves (which are *usually* “V” shaped). Finally, the additional candidates have durations that can be explained by orbiting the same stars as the confirmed planets (Fig. 1). Despite the fainter target stars which makes formal validation difficult, we expect most if not all of these candidates are indeed planets.

Funding for this mission is provided by NASA’s Science Mission Directorate. We thank the entire *Kepler* team for the many years of work that is proving so successful. We thank E. Agol for comments and G. Sokol for assistance analyzing starspot variations. D. C. F. and J. A. C. acknowledge support for this work was provided by NASA through Hubble Fellowship grants #HF-51272.01-A and #HF-51267.01-A awarded by the Space Telescope Science Institute, which is operated by the Association of Universities for Research in Astronomy, Inc., for NASA, under contract NAS 5-26555. E.B.F acknowledges support by the National Aeronautics and Space Administration under grant NNX08AR04G issued through the Kepler Participating Scientist Program. This material is based upon work supported by the National Science Foundation under Grant No. 0707203. This paper uses observations obtained with facilities of the Las Cumbres Observatory Global Telescope.

Facilities: Kepler.

Table 1
Properties of target stars

	KOI	KIC-ID	K _p	C0 ^a	C1 ^a	C2 ^a	C3 ^a	CDPP ^b [ppm]	RA hr [J2000]	DEC deg [J2000]
Kepler-29	738	10358759	15.282	0.108	0.054	0.091	0.092	176	19 53 23.60	+47 29 28.4
Kepler-30	806	3832474	15.403	0.094	0.099	0.116	0.056	652	19 01 08.07	+38 56 50.2
Kepler-31	935	9347899	15.237	0.053	0.045	0.119	0.063	186	19 36 05.52	+45 51 11.1
Kepler-32	952	9787239	15.913	0.096	0.117	0.193	0.119	288	19 51 22.18	+46 34 27.4

Note. — Information mostly from the *Kepler* Input Catalog.

^a Contamination for each season 0-3 (season = (quarter+2) mod 4):
the fractional amount of light leaking in to the target's aperture from
other stars, known from the *Kepler* Input Catalog.

^b Combined differential photometric precision on 6 hour timescales.

Table 2
Table of Stellar Properties of Hosts

	T_{eff} (K)	$\log g$ (cgs)	$v \sin i$ (km s ⁻¹)	[Fe/H]	M_{\star} M_{\odot}	R_{\star} R_{\odot}
Kepler-29	5750 ± 250 (L)	5.00 ± 0.25 (L)	4 ± 2 (L)	0.0 ± 0.3 (N)	1.00±0.12	0.96±0.14
Kepler-30	5498 ± 54 (K)	4.77 ± 0.23 (K)	1.94 ± 0.22 (K)	0.18 ± 0.27 (K)	0.99±0.08	0.95±0.12
Kepler-31	6340 ± 200	4.696 ± 0.300		-0.076 ± 0.400	1.21±0.17	1.22±0.24
Kepler-32	3900 ± 200 (K,M)	4.64 ± 0.30		0 ± 0.4	0.58 ± 0.05	0.53 ± 0.04

^a Sources for stellar properties. Spectroscopic parameter with un-
certainties indicated in parentheses are from: K=Keck Observatory,
L=Lick Observatory, M=McDonald Observatory, N=NOAO. Quoted
uncertainties do not include systematic uncertainties due to stellar
models.

Table 3
Key Properties of Planets and Planet Candidates

	T_0^a (d)	P^b (d)	T_{Dur}^c (d)	b^d	u^d	Depth (ppm)	R_p/R_* ^e	R_p^f R_\oplus	a (AU)	$M_{p,\text{max}}^g$ M_{Jup}
29b	82.750±0.009	10.3376±0.0002	0.117±0.003	0.0 – 0.85	0.0 – 0.5	1152	0.0343±0.0008	3.6±0.5	0.09	0.4
29c	78.471±0.016	13.2907±0.0004	0.127±0.006	928	0.0280±0.0012	2.9±0.4	0.11	0.3
30b	83.04±0.41	29.329±0.022	0.200±0.004	1115	0.0351±0.0005	3.7±0.5	0.18	0.2
30c	176.904±0.005	60.3251±0.0008	0.2392±0.0011	0.44±0.04	0.584±0.023	19862	0.1375±0.0011	14.4±1.8	0.30	9.1
30d	87.220±0.038	143.213±0.013	0.322±0.003	0.52±0.04	0.56±0.05	10175	0.1020±0.0014	10.7±1.4	0.5	17
935.04	85.10±0.04	9.6172±0.0005	0.176±0.014	...	0 – 0.6	196	0.0136±0.0006	1.3±0.3	0.09	...
31b	92.141±0.006	20.8613±0.0002	0.208±0.002	0 – 0.75	0.38 – 0.70	1942	0.0411±0.0006	4.3±0.8	0.16	...
31c	74.191±0.007	42.6318±0.0005	0.251±0.004	0 – 0.8	0.18 – 0.67	1764	0.0400±0.0007	4.2±0.8	0.26	4.7
935.03	67.942±0.009	87.6451±0.0014	0.344±0.010	0 – 0.9	0.1 – 1.0	1035	0.0291±0.0011	3.1±0.7	0.4	6.8
952.05	65.54±0.04	0.74296±0.00007	0.039±0.004	215	0.0142±0.0007	1.5±0.1	0.013	...
952.04	66.61±0.03	2.8960±0.0003	0.053±0.004	1642	0.0259±0.0013	2.7±0.2	0.033	...
32b	74.902±0.008	5.90124±0.00010	0.088±0.005	1579	0.0389±0.0019	4.1±0.4	0.05	4.1
32c	77.378±0.013	8.7522±0.0003	0.097±0.010	1897	0.0352±0.0033	3.7±0.4	0.09	0.5
952.03	88.211±0.011	22.7802±0.0005	0.124±0.003	...	0.0 – 0.75	385	0.0467±0.0011	4.9±0.4	0.13	...

^a BJD-2454900. Rather than statistical error bars, we report the RMS of the measured transit timing deviations.

^b Derived from the measured transit times. Error bar is the RMS of the measured transit timing deviations, divided by the number of transits that the data span.

^c Duration of time that the center of the planet overlies the stellar disk.

^d Values with \pm error bars are from formal fits. However, often we found b and u to be quite poorly constrained and/or degenerate, so we computed grids in b , $u \in [0, 1]$, and give either a $2\text{-}\sigma$ ($\Delta\chi^2 = 4$) range, or if this range covers the whole grid, no value at all.

^e Takes into account contamination values from Table 1.

^f Using stellar radii from Table 2.

^g Based on assumption of dynamical stability and stellar mass from Table 2.

Table 4
Table of Statistics for Pairs of Planets Candidates

KOI _{in}	frequency _{in}	FAP _{in}	KOI _{out}	frequency _{out}	FAP _{out}
Kepler-29b	0.00026034	0.00018	Kepler-29c	0.00026086	0.01513
Kepler-30b	0.00094237	$< 10^{-5}$	Kepler-30c	0.00095528	$< 10^{-5}$
Kepler-30b	0.00698565	0.55100	Kepler-30d	0.00082395	0.30800
Kepler-30c	0.00259824	0.00400	Kepler-30d	0.00262702	$< 10^{-5}$
Kepler-31b	0.00100550	$< 10^{-5}$	Kepler-31c	0.00100732	0.03360
Kepler-31b	0.01140540	0.53060	935.03	0.00229586	0.96650
Kepler-31c	0.00064850	0.02580	935.03	0.00064007	0.13400
952.04	0.00642701	0.11427	Kepler-32b	0.00642994	0.27161
952.04	0.11678254	0.09436	Kepler-32c	0.00252686	0.16165
952.04	0.04389705	0.51453	952.03	0.00587133	0.61985
Kepler-32b	0.00390700	0.00001	Kepler-32c	0.00391415	0.05363
Kepler-32b	0.04389928	0.84870	952.03	0.00613203	0.49878
Kepler-32c	0.02646319	0.87862	952.03	0.01743588	0.65570
Kepler-9b	0.00066337	0.00002	Kepler-9c	0.00066211	0.00170
Kepler-18c	0.00373946	$< 10^{-5}$	Kepler-18d	0.00381809	$< 10^{-5}$
168.02	0.02919133	0.80572	Kepler-23b	0.02919325	0.80219
168.02	0.01021819	0.37630	Kepler-23c	0.01022921	0.65446
Kepler-23b	0.00215313	0.00084	Kepler-23c	0.00214191	$< 10^{-5}$
1102.04	0.00994495	0.22250	1102.02	0.00994282	0.35748
1102.04	0.07345063	0.75543	1102.01	0.00762697	0.91916
1102.04	0.05264294	0.25841	1102.03	0.02506453	0.56294
Kepler-24b	0.00237619	$< 10^{-5}$	Kepler-24c	0.00237709	$< 10^{-5}$
Kepler-24b	0.01749593	0.85933	1102.03	0.01752736	0.14017
Kepler-24c	0.00424632	0.63164	1102.03	0.00424409	0.57523
Kepler-25b	0.00305506	$< 10^{-5}$	Kepler-25c	0.00306491	0.02136
250.03	0.11935114	0.02223	Kepler-26b	0.03794286	0.84931
250.03	0.05797149	0.06283	Kepler-26c	0.00765104	0.10796
Kepler-26b	0.01119109	0.05656	Kepler-26c	0.01118508	0.28181
Kepler-27b	0.00137000	0.00061	Kepler-27c	0.00137385	0.00083
Kepler-28b	0.00426232	$< 10^{-5}$	Kepler-28c	0.00429017	0.00239

Note. — Theoretically predicted O-C frequencies are in cycles per day. False Alarm Probabilities (FAP) are bold, if the detection is considered significant ($FAP < 10^{-3}$). Systems above the line are presented as planetary system discoveries in this paper. Systems below the double horizontal line are presented as planetary system discoveries in Holman et al. (2010), in Cochran et al. (2011), and in the companion papers, papers II and III.

Table 5
Example TTV Solution for Planets Candidates

system $M_\star (M_\odot)$	planet	P (days)	T_0 BJD-2454900	$e \cos \omega$	$e \sin \omega$	M_p (formal, M_\oplus)	M_p (3- σ upper- limit, M_\oplus)	χ^2 / d.o.f.
Kepler-23 1.21	b	7.107977 ± 0.000934	320.024941 ± 0.007984	0.030090 ± 0.454676	-0.061653 ± 0.357376	4.8 ± 15.6	80	112.1 / 65
	c	10.741598 ± 0.001250	324.116640 ± 0.002704	0.034012 ± 0.386216	-0.056846 ± 0.294888	15.0 ± 49.8	700	38.2 / 44
Kepler-24 1.10	b	8.163886 ± 0.004031	326.108132 ± 0.005328	-0.336422 ± 0.090501	0.238848 ± 0.117101	56.1 ± 15.8	130	86.3 / 70
	c	12.315302 ± 0.003671	329.547776 ± 0.006364	-0.267037 ± 0.082641	0.202843 ± 0.099609	102.8 ± 21.4	350	131.7 / 45
Kepler-25 1.10	b	6.238383 ± 0.000100	323.057366 ± 0.000547	-0.011764 ± 0.002010	-0.007540 ± 0.003149	8.1 ± 3.1	310	83.4 / 74
	c	17.250640 ± 0.000179	327.772432 ± 0.000337	-0.029885 ± 0.006415	-0.020024 ± 0.003600	13.3 ± 3.9	30	43.9 / 36
Kepler-26 0.55	b	12.281204 ± 0.000580	324.486687 ± 0.000982	-0.009929 ± 0.018073	-0.360464 ± 0.366736	2.0 ± 1.0	4.6	65.1 / 35
	c	17.253059 ± 0.001135	324.406889 ± 0.001088	-0.017962 ± 0.015168	-0.317353 ± 0.316959	3.9 ± 1.4	20	25.4 / 24
Kepler-27 0.94	b	15.337102 ± 0.002742	321.703954 ± 0.001715	0.015924 ± 0.010802	0.000148 ± 0.001418	28.5 ± 12.6	800	34.3 / 30
	c	31.330788 ± 0.000717	337.066843 ± 0.001887	0.032298 ± 0.026605	0.003735 ± 0.009598	51.4 ± 43.7	260	20.2 / 15
Kepler-28 0.89	b	5.911764 ± 0.000426	323.929704 ± 0.002061	-0.050253 ± 0.175120	-0.075099 ± 0.469131	3.8 ± 6.9	320	54.4 / 75
	c	8.986416 ± 0.000612	324.352707 ± 0.002432	-0.020126 ± 0.139930	-0.078354 ± 0.376697	4.9 ± 9.3	50	93.3 / 50
Kepler-29 1.05	b	10.335908 ± 0.001440	320.506863 ± 0.002675	-0.049991 ± 0.035113	-0.039249 ± 0.033556	2.8 ± 2.4	8.2	42.5 / 46
	c	13.293451 ± 0.001333	331.005742 ± 0.003308	-0.008036 ± 0.014426	-0.050000 ± 0.000000	2.3 ± 2.0	5.4	54.4 / 34
Kepler-30 0.99	b	29.221698 ± 0.003828	346.363743 ± 0.007351	0.100465 ± 0.008802	0.067662 ± 0.015178	4.0 ± 0.5	8.5	73.2 / 18
	c	60.328168 ± 0.000441	357.884196 ± 0.000584	0.032345 ± 0.006953	-0.019980 ± 0.003602	219.2 ± 28.4	490	18.4 / 9
	d	143.332307 ± 0.016328	373.632984 ± 0.003042	-0.034437 ± 0.008653	-0.073924 ± 0.013089	30.7 ± 3.6	56	0.048 / 4
Kepler-31 1.09	b	20.856113 ± 0.002883	321.610535 ± 0.002182	0.007721 ± 0.003806	-0.000270 ± 0.005266	18.4 ± 35.5	140	27.8 / 30
	c	42.637618 ± 0.009447	329.984885 ± 0.002964	-0.001835 ± 0.015429	0.031462 ± 0.034318	34.9 ± 21.2	120	13.9 / 13
Kepler-32 0.49	b	5.900841 ± 0.000188	322.747894 ± 0.001616	-0.003717 ± 0.008006	-0.000888 ± 0.001491	7.2 ± 4.1	24	97.7 / 76
	c	8.752819 ± 0.000545	322.449605 ± 0.002362	0.001713 ± 0.002330	0.001658 ± 0.001150	5.2 ± 3.5	18	70.8 / 52

Note. — A sample of TTV-fit results for each system presented here.

Table 6
Transit Times for Kepler Transiting Planet Candidates

KOI	n	t_n BJD-2454900	TTV _n (d)	σ_n (d)
738.01		$82.749505 + n \times 10.337583$		
738.01	0	82.7642	0.0147	0.0081
738.01	1	93.1033	0.0162	0.0074

Note. — Table 6 is published in its entirety in the electronic edition of the *Astrophysical Journal* or from the “tttable” within the source files of this arxiv posting. A portion is shown here for guidance regarding its form and content.

REFERENCES

Agol, E., Steffen, J., Sari, R., & Clarkson, W. 2005, MNRAS, 359, 567
 Barnes, R., & Greenberg, R. 2006, ApJ, 647, L163
 Bonomo, A. S., Hébrard, G., Santerne, A., et al. 2011, preprints (arxiv:1110.5462)
 Borucki, W. J., Koch, D. G., Basri, G., et al. 2011, ApJ, 736, 19
 Bouchy, F., Bonomo, A. S., Santerne, A., et al. 2011, A&A, 533, A83
 Brown, T. M., Latham, D. W., Everett, M. E., & Esquerdo, G. A. 2011, AJ, 142, 112
 Chambers, J. E. 1999, MNRAS, 304, 793
 Chambers, J. E., Wetherill, G. W., & Boss, A. P. 1996, Icarus, 119, 261
 Chatterjee, S., Ford, E. B., Matsumura, S., & Rasio, F. A. 2008, ApJ, 686, 580
 Cochran, W. D., Fabrycky, D. C., Torres, G., et al. 2011, ApJS, 197, 7
 Cohen, C. J., & Hubbard, E. C. 1965, AJ, 70, 10
 Demory, B.-O., & Seager, S. 2011, ApJS, 197, 12
 Désert, J.-M., Charbonneau, D., Demory, B.-O., et al. 2011, ApJS, 197, 14
 Desort, M., Lagrange, A.-M., Galland, F., et al. 2008, A&A, 491, 883
 Doyle, L. R., Carter, J. A., Fabrycky, D. C., et al. 2011, Science, 333, 1602
 Duncan, M., Quinn, T., & Tremaine, S. 1989, Icarus, 82, 402
 Duncan, M. J., & Lissauer, J. J. 1997, Icarus, 125, 1
 Duquennoy, A., & Mayor, M. 1991, A&A, 248, 485
 Edelson, R. A., & Krolik, J. H. 1988, ApJ, 333, 646
 Fabrycky, D. C. 2010, Non-Keplerian Dynamics of Exoplanets (University of Arizona Press), 217–238
 Fabrycky, D. C., & Murray-Clay, R. A. 2010a, ApJ, 710, 1408
 —. 2010b, ApJ, 710, 1408
 Ford, E. B., Fabrycky, D. C., & Steffen, J. H. 2012, accepted to ApJ (Paper II)
 Ford, E. B., Rowe, J. F., Fabrycky, D. C., et al. 2011, ApJS, 197, 2
 Fortney, J. J., Marley, M. S., & Barnes, J. W. 2007, ApJ, 659, 1661
 Fressin, F., Torres, G., Désert, J.-M., et al. 2011, ApJS, 197, 5
 García-Melendo, E., & López-Morales, M. 2011, MNRAS, 417, L16
 Girardi, L., Bertelli, G., Bressan, A., et al. 2002, A&A, 391, 195
 Gladman, B. 1993, Icarus, 106, 247
 Holman, M. J., Fabrycky, D. C., Ragozzine, D., et al. 2010, Science, 330, 51
 Howard, A. W., Marcy, G. W., Bryson, S. T., et al. 2011, ArXiv e-prints
 Ida, S., & Lin, D. N. C. 2010, ApJ, 719, 810
 Jenkins, J. M., Caldwell, D. A., Chandrasekaran, H., et al. 2010, ApJ, 713, L87
 Johnson, J. A., Gazak, J. Z., Apps, K., et al. 2011, ArXiv e-prints
 Laskar, J., & Correia, A. C. M. 2009, A&A, 496, L5

Latham, D. W., Rowe, J. F., Quinn, S. N., et al. 2011, ApJ, 732, L24
 Lissauer, J. J., Fabrycky, D. C., Ford, E. B., et al. 2011a, Nature, 470, 53
 Lissauer, J. J., Ragozzine, D., Fabrycky, D. C., et al. 2011b, ApJS, 197, 8
 Liu, H., Zhou, J.-L., & Wang, S. 2011, ApJ, 732, 66
 Malhotra, R., Black, D., Eck, A., & Jackson, A. 1992, Nature, 356, 583
 Mandel, K., & Agol, E. 2002, ApJ, 580, L171
 Marchal, C., & Bozis, G. 1982, Celestial Mechanics, 26, 311
 Marois, C., Zuckerman, B., Konopacky, Q. M., Macintosh, B., & Barman, T. 2010, Nature, 468, 1080
 Masset, F., & Snellgrove, M. 2001, MNRAS, 320, L55
 Mayor, M., Udry, S., Lovis, C., et al. 2009, A&A, 493, 639
 McNeil, D. S., & Nelson, R. P. 2010, MNRAS, 401, 1691
 Morbidelli, A., Tsiganis, K., Crida, A., Levison, H. F., & Gomes, R. 2007, AJ, 134, 1790
 Muirhead, P. S., Hamren, K., Schlawin, E., et al. 2011, preprint (arxiv:1109.1819)
 Mustill, A. J., & Wyatt, M. C. 2011, MNRAS, 413, 554
 Nobili, A., & Roxburgh, I. W. 1986, in IAU Symposium, Vol. 114, Relativity in Celestial Mechanics and Astrometry. High Precision Dynamical Theories and Observational Verifications, ed. J. Kovalevsky & V. A. Brumberg, 105–110
 Nutzman, P. A., Fabrycky, D. C., & Fortney, J. J. 2011, ApJ, 740, L10
 Peale, S. J. 1993, AJ, 105, 1562
 Pepe, F., Lovis, C., Ségransan, D., et al. 2011, A&A, 534, A58
 Pierens, A., Baruteau, C., & Hersant, F. 2011, A&A, 531, A5+
 Pierens, A., & Nelson, R. P. 2008, A&A, 482, 333
 Pont, F., & Eyser, L. 2004, MNRAS, 351, 487
 Queloz, D., Bouchy, F., Moutou, C., et al. 2009, A&A, 506, 303
 Raghavan, D., McAlister, H. A., Henry, T. J., et al. 2010, ApJS, 190, 1
 Rasio, F. A., Nicholson, P. D., Shapiro, S. L., & Teukolsky, S. A. 1992, Nature, 355, 325
 Raymond, S. N., & Barnes, R. 2005, ApJ, 619, 549
 Rein, H., & Papaloizou, J. C. B. 2010, in EAS Publications Series, Vol. 42, EAS Publications Series, ed. K. Goździewski, A. Niedzielski, & J. Schneider, 299–302
 Rivera, E. J., Laughlin, G., Butler, R. P., et al. 2010, ApJ, 719, 890
 Robin, A. C., Reylé, C., Derrière, S., & Picaud, S. 2003, A&A, 409, 523
 Sanchis-Ojeda, R., Winn, J. N., Holman, M. J., et al. 2011, ApJ, 733, 127
 Santerne, A., Bonomo, A. S., Hébrard, G., et al. 2011a, A&A, 536, A70
 Santerne, A., Díaz, R. F., Bouchy, F., et al. 2011b, A&A, 528, A63
 Scargle, J. D. 1982, ApJ, 263, 835
 Schlichting, H. E., & Chang, P. 2011, ApJ, 734, 117
 Steffen, J. H., Ford, E. B., & Fabrycky, D. C. 2012, submitted to MNRAS (Paper III)
 Takeda, G., Ford, E. B., Sills, A., et al. 2007, ApJS, 168, 297
 Terquem, C., & Papaloizou, J. C. B. 2007, ApJ, 654, 1110
 Thommes, E. W., Bryden, G., Wu, Y., & Rasio, F. A. 2008, ApJ, 675, 1538
 Tingley, B., Palle, E., Parviainen, H., et al. 2011, preprint (arxiv:1111.5107)
 Torres, G., Fressin, F., Batalha, N. M., et al. 2011, ApJ, 727, 24
 Valenti, J. A., & Fischer, D. A. 2005, ApJS, 159, 141
 Valenti, J. A., & Piskunov, N. 1996, A&AS, 118, 595
 White, R. J., & Peterson, B. M. 1994, PASP, 106, 879
 Wisdom, J. 1980, AJ, 85, 1122
 Wisdom, J., & Holman, M. 1991, AJ, 102, 1528
 Wolszczan, A. 1994, Science, 264, 538
 Yi, S., Demarque, P., Kim, Y.-C., et al. 2001, ApJS, 136, 417
 Zechmeister, M., & Kürster, M. 2009, A&A, 496, 577
 Zhou, J.-L., Lin, D. N. C., & Sun, Y.-S. 2007, ApJ, 666, 423